Washington University in St. Louis

Washington University Open Scholarship

January 2011

Markov Chains Derived From Lagrangian Mechanical Systems

Scott Cook
Washington University in St. Louis

WASHINGTON UNIVERSITY

Department of Mathematics

Dissertation Examination Committee:

Renato Feres, Chair

Rachel Roberts

Alexander Seidel

John Shareshian

Xiang Tang

Gregory Yablonsky

MARKOV CHAINS DERIVED FROM LAGRANGIAN MECHANICAL SYSTEMS

by

Scott A. Cook

A dissertation presented to the

Graduate School of Arts and Sciences

of Washington University in

partial fulfillment of the

requirements for the degree

of Doctor of Philosophy

May 2011

St. Louis, Missouri

To μ, χ, and ζ

ACKNOWLEDGMENTS

First, I would like to thank my two advisors Renato Feres and John Shareshian for all they have done to make this dream a reality. To Prof. Feres, you have been so generous with your time and attention. Your talent and class are matched only by your skill as a mentor. To Prof. Shareshian, thank you all the support along the way. Your continued belief in me has helped me keep pushing forward and your sage advice has put me on the right path. In particular, thank you for the chance to visit MSRI. You have both helped me to grow as a mathematician and as a human. Thank you.

Furthermore, I would like to thank Rachel Roberts, Xiang Tang, Gregory Yablonsky, and Alexander Seidel for their contributions to this dissertation. I would also like to thank the Washington University Mathematics Department for providing a wonderful place to do mathematics and support to go do it elsewhere too.

To my wife Megan, how can I thank you for the support and patience you have given me? It made the difference between success and failure. We made it!

I'd like to thank Drew Lewis for being a great office mate, a willing conversant (mathematically and otherwise), and an invaluable source of tech support.

I'd like to thank my friends here in St. Louis who have helped to keep me sane(ish) - Andy Womack, Drew Lewis, Josh Brady, Brad Henry, Nic Sedlock, Mike Deutsch,

TABLE OF CONTENTS

1. Introduction

The theory of Markov chains with countable state spaces is a greatly developed and successful area of probability theory and statistics. There is much interest in continuing to develop the theory of Markov chains beyond countable state spaces. One needs good and well motivated model systems in this effort. In this thesis, we propose to produce such systems by introducing randomness into familiar deterministic systems so that we can draw upon the existing (deterministic) results to aid the analysis of our Markov chains. We will focus most heavily on models drawn from Lagrangian mechanical systems with collisions (billiards).

In this chapter, we will give a detailed introduction to a broad framework called measured fibrations we have developed for thinking about these systems, introduce some elements of Lagrangian mechanics from which we draw our main model, state and take substantial steps in the proof of the main results of the thesis, and show how this area of study integrates with the wider mathematical landscape.

1.1   General Framework

The broad objective of this work is to generate general state Markov chains from deterministic systems, such as mechanical systems with collisions. Our primary technique for converting deterministic systems into probabilistic systems is to separate

quantities into "observable" and "hidden" types. The "hidden" variables will be treated as random, making the entire system probabilistic.

As a motivating example, figure 1.1 shows a single gas particle traveling inside a long two dimensional tube. The interior surface of this tube is slightly rough. This <u>microstructure</u> causes the particle to scatter upon impact with the tube. This scattering is thoroughly deterministic; the angle of reflection is easily computable given the angle of incidence and the point of impact on the microstructure. Observe that a small difference in the point of impact makes a substantial difference in the angle of reflection.
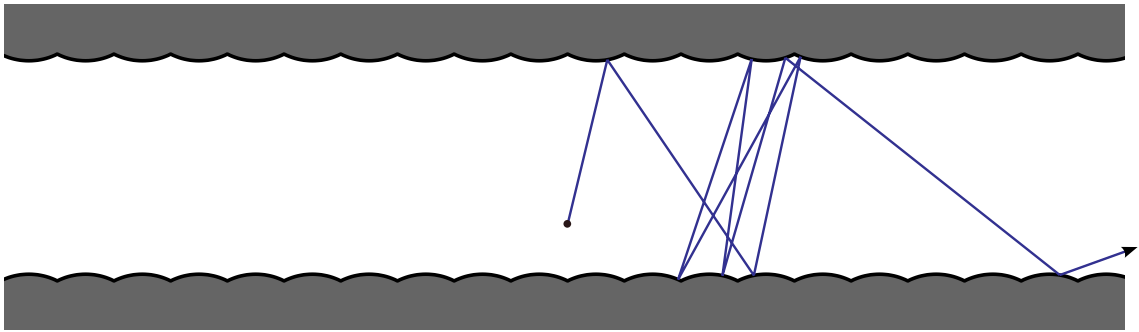
Figure 1.1. Tube with microstructure

We assume that the dimensions of the microstructure are very small relative to the dimensions of the tube itself (for display purposes, we have magnified the microstructure in the figure). So, an observer at the size scale of the tube sees an essentially smooth surface. In other words, she cannot resolve the point of impact with sufficient precision to deterministically predict the outcome of an impact. We say that the point

2

of impact is a *hidden* variable to this observer, so that she has *partial knowledge* of the system. Thus, she sees the particle bouncing quite erratically off an apparently smooth surface even though an observer at the size scale of the microstructure can see that the reflections are perfectly deterministic. Note that both observers can see the angle of incidence, so we say this variable is *observable*.

1.1.1   Measured Fibrations

We have developed a language for thinking about such models. Let U and B be measure spaces, $\pi : U \to B$ a surjective measurable map, and $F : U \to U$ an invertible measureable map. A point $u \in U$ represents perfect knowledge of all quantities associated to the current state of the system and F determines the next state of the system given this knowledge. The map π "hides" some information contained in u; in other words, $\pi(u)$ represents the partial knowledge available to the observer.

Thus, B represents the observable variables. If the system is observed to be at $b \in B$, its "true" state is somewhere in $\pi^{-1}(b)$, called the <u>fiber over b</u>. So, on each fiber, we fix a probability measure η_b to encode this distribution and call $(\eta_b)_{b \in B}$ the <u>probability kernel</u>. Let $\mathscr{P}(X)$ denote the space of probability measures on X.

The proper notion of the observable state of the system is a probability measure $\nu \in \mathscr{P}(B)$. If an observation is made and outcome is b, we say that the system is temporarily at δ_b, the delta measure at b. However, the next step of the process

involves random choices for the hidden variables, so that the support of the measure increases (it "spreads out"). We now describe the evolution of the system.

Given $\nu \in \mathscr{P}(B)$, define its lift to U by

$$(\nu \circ \eta)(f) := \int_B \int_{u \in \pi^{-1}(b)} f(u) d\eta_b(u) d\nu(b) \tag{1.1}$$

where $f : U \to \mathbb{R}$ is measurable. So, we only allow choices of $(\eta_b)_{b \in B}$ where this definition gives a well-defined measure on U (Fubini's theorem applies). Then we define the Markov operator for the system:

$$P : \nu \mapsto \pi_*(F_*(\nu \circ \eta)) \tag{1.2}$$

where π_* and F_* are the pushforward maps of π and F. Thus, we have

$$(\nu P_\eta)(g) = (\nu \circ \eta)(g \circ \pi \circ F) = \int_B \int_{\pi^{-1}(b)} f((\pi \circ F)(u)) d\eta_b(u) d\nu(b) \tag{1.3}$$

for $g : B \to \mathbb{R}$ measurable. We say ν is P-stationary if

$$\nu P = \nu$$

noting that we abide the usual convention that P operates on measures from the right and on functions from the left.

We call this setup a <u>measured fibration</u>. It provides a convenient language for producing Markov chains from deterministic systems. In chapter 2, we will establish some basic results about measured fibrations which will aid the analysis of the specific gas-surface interaction model which we wish to investigate; much more can be said.

Recall that a measure $\mu \in \mathscr{P}(U)$ is said to be F-invariant if the pushforwrd $F_*\mu = \mu$. We will show that if μ is F-invariant and $\mu = \nu \circ \eta$, then ν is P-stationary.

$$U \xrightarrow{\; F \;} U$$

$$\pi \Big\downarrow \qquad \Big\downarrow \pi \qquad \nu \mapsto \nu P := (\pi \circ F)_* \nu \circ \eta$$

$$B \underset{\text{random map}}{\longrightarrow} B$$

Figure 1.2. A Measured Fiber Bundle

Once a stationary ν is identified, we have the Hilbert space $L^2(B, \nu)$. We will see that P is a bounded operator of norm 1 on this space.

We can say more by imposing additional symmetry. For example, a natural symmetry is time reversibility which will be used to produce a map J such that the adjoint $P^* = J^* P J$. If we further impose a type of bilateral symmetry (note the "bumps" in figure 1.1 are symmetric w.r.t the perpendicular bisector), we show that J and P commute, so that P is self-adjoint. This implies that the spectrum of P is real and contained in $[-1, 1]$. Recall that the spectrum of P can often be used to estimate rates of convergence for the Markov chain.

In the example of figure 1.1, the stationary distribution ν is known. Thus, one can proceed directly to the investigation of spectrum, as in [1]. However, we wish to apply the idea of "hiding" variables to produce Markov chains in more complicated circumstances as well. In such cases, the stationary distribution may not be obvious; this is the case for the gas-surface interaction model with moving parts explored in the body of this thesis. Thus, a primary focus of this thesis will be on establishing ν for this model using Lagrangian mechanics.

To make this more concrete, note that any countable state Markov chain can be seen in this framework; the measured fibration framework is equivalent to a *random mapping representation*, see [2].

For a very concrete example, take the simple random walk on the n-cycle, and let

$$B = \mathbb{Z}_n$$

$$U = \mathbb{Z}_n \times \{-1, 1\}$$

$$\pi(z, a) = z$$

$$F(z, a) = z + a \mod n$$

More generally, an arbitrary countable state Markov chain can be nicely set into this context using the notion of a groupoid. The advantage of using the groupoid structure is that the dynamical map F takes a concrete form. Groupoids are a way to generalize the notion of a group action on a set, with the restriction that not all maps can be composed. We introduce the groupoid perspective solely as an example; it will not play an explicit role going forward, so we will leave some of the measure theoretic details unstated.

Fix a base set X and a set of maps $\mathscr{G}$. An element $g \in \mathscr{G}$ has a source $s(g) \subset X$ of elements on which it acts and a range $r(g) \subset X$ of elements to which it maps some element of its range. Then we can multiply g_1 and g_2 iff $r(g_1) = s(g_2)$. In fact, we denote $\mathscr{G}_1 \subset \mathscr{G} \times \mathscr{G}$ to be the sets of ordered pars that can be multiplied. We insist that each element have an inverse g^{-1} such that $r(g) = s(g^{-1})$, $r(g^{-1}) = s(g)$, and $g \cdot g^{-1}$ and $g^{-1} \cdot g$ are the identity maps on their sources.

Then consider the

$$B = X$$

$$U = X \times \mathcal{G}$$

$$\pi(x, g) = x$$

and when $x \in s(g)$, define $\iota(x, g) = (g(x), g^{-1})$.

Now, for each $x \in X$, choose a measure η_x on $\mathcal{G}_x := \{g : x \in s(g)\}$ (the set of maps that act on x). This produces a measured fiber bundle where the dynamical map has the concrete form ι.

We can see countable Markov chains in this way. Let X be the state space of the chain and let $\mathcal{G}$ be all ordered pairs of states and $U = X \times \mathcal{G}$. Then $g = (x, y)$ is the map $s(g) = \{x\}, r(g) = \{y\}, x \mapsto y$. So the probabilty kernel is defined by

$$\eta_x((\bar{y}, y)) = \begin{cases} Pr(x \to y), & \text{if } \bar{y} = x \\ \\ 0, & \text{if } \bar{y} \neq x \end{cases}$$

Then a measure ν on V evolves under $\pi_*(\iota_*(\nu \circ \eta))$ in the manner familiar from Markov chains. In particular, denoting δ_x, to be delta measure at x, we see

$$(\delta_x P_\eta)(f) = (\delta_x \circ \eta)(f \circ \pi \circ \iota)$$

$$= \int_{\mathcal{G}} f((\pi \circ \iota)(g)) d\eta_x(g)$$

$$= \sum_{y \in X} f(y) Pr(x \to y)$$

In this thesis, we will look to mechanical systems as the source of systems to make random. However, the idea extends much more broadly. For example, consider the recent work in the mathematics of card shuffling, such in [3, 4]. Let B be the unit interval and let each step of the Markov chain begin with a random choice of a number of "cards" into which B is divided. Then shuffle the interval as a deck of cards, thus producing a Markov chain on the set of bijections of the interval.

1.2 Lagrangian Mechanics

In this section, we provide a very brief introduction to mechanics; see [5] for more background. We will then introduce several examples of mechanical systems that fit into our framework, paying particular attention to elements we need to work on the gas-surface interaction model with moving parts.

1.2.1 Background to Lagrangian Mechanics

Let X be a smooth manifold of dimension n endowed with a Riemannian metric $\langle \cdot, \cdot \rangle$. The norm of a vector v in the tangent space $T_p X$ at $p \in X$ is written $||v||_p$. We assume that the boundary ∂X is a non-empty, piecewise smooth submanifold and denote by $\mathbf{n}$ the unit normal vector field on ∂X.

We select a subset $S \subset \partial X$ consisting of a finite number of boundary components to represent the "interface" of X with the "macroscopic world". In some of the examples below, we consider a particle (or other rigid body) moving through an

8

ambient space until it reaches S. At S, the particle enters the "microscopic world"

of X, where its motion is governed by deterministic mechanical laws until it returns

to S. Entry into X through S involves the random choice of the values of "hidden"

variables and exit out of X through S requires the system to forget this information.

At the other boundary components, the particle experiences specular reflection

$$C(p, v) := v - 2\langle v, \mathbf{n}(p)\rangle\mathbf{n}(p) \tag{1.4}$$

We assume that S has finite volume (w.r.t. the Riemannian volume form) and

carries a measurable orthonormal frame $e_1(p), ..., e_{n-1}(p)$ on S, so at each $p \in S$, they

form an orthonormal basis of T_pS. Let $e_n(p) = \mathbf{n}(p)$ (recall $\mathbf{n}$ is the inward pointing

normal vector). We assume these vector fields are well-defined and smooth on an

open, dense set of full measure.

Let $V : X \to \mathbb{R}$ be a smooth function — the potential function for the system —

and define the Lagrangian $L : TX \to \mathbb{R}$ to be the real valued function on the tangent

bundle given by:

$$L(p, v) := \frac{1}{2}||v||_p^2 - V(p)$$

Thus the square of the Riemannian norm specifies the *kinetic energy* of the system in

the *kinetic state* represented by (p, v). For convenience, we assume that V is bounded

on S and without loss of generality, globally substract its minimal value on S.

The time evolution of the system for a given initial state (i.e. a point in TX)

is given by the *Hamiltonian flow*, defined by the one-parameter group of diffeomor-

phisms of TX denoted $\{\Phi_t : t \in \mathbb{R}\}$.

The trajectories of the Hamiltonian flow in TX projects to curves on X that satisfy Newton's equation

$$\frac{\nabla \gamma'}{dt} = -\text{grad } V$$

where the left-hand side represent covariant acceleration (in terms of the Levi-Civita connection ∇) of a path $\gamma(t)$ in X. When the potential funtion V is constant, the Hamiltonian flow corresponds to geodesic flow of X, extended to include specular reflection at boundary components.

The *energy function* or *Hamiltonian* of the system is the function $E : TX \rightarrow \mathbb{R}$ given by

$$E(p, v) := \frac{1}{2}||v||_p^2 + V(p)$$

When convenient, we omit the base point p. We also denote

$$r(p, v) := 2\sqrt{E(p, v)}$$

which represents speed in the case of zero potential. It is easy to show that E is invariant under Φ_t, so it makes sense to (for the moment) restrict this flow to the constant energy level sets $N_r := T^r X$ where $E \equiv \frac{1}{2}r^2$. We are particularly interested in

$$W_r := \{(p, v) : p \in S, E(p, v) = \frac{1}{2}r^2, \text{ and } \langle v, \mathbf{n} \rangle > 0\}$$

Thus, W_r is a piecewise smooth manifold of dimension $2n - 2$ whose points represent states of entry into X having energy $\frac{1}{2}r^2$ and position configuration represented by a point in S.

One fundamental property of Hamiltonian flows is that they preserve a volume measure called the *Liouville measure* on N_r. We assume that the total Liouville measure of N_r is finite for all r. In the special case of constant potential V, this is equivalent to the assumption that X has finite volume.

The Liouville measure is induced by a $(2n-1)$-form on N_r. A related $(2n-2)$-form denoted Ω_r (described later) can also be defined on W_r. To Ω_r, we associate a measure μ_r on W_r which we also assume to be finite. Thus, we may normalize so that the total measure is 1 and μ_r is a probability measure on W_r.
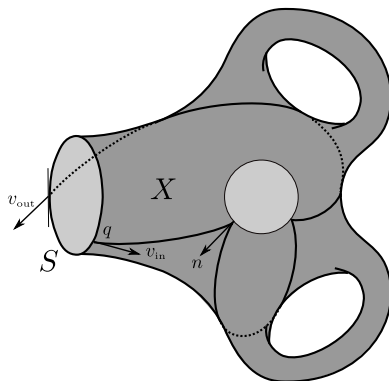
Figure 1.3. The return map sends v_{in} in N to the image of v_{out} under the reflection map through the tangent space of S at the return point. The trajectory with initial state v_{in} satisfies Newton's equations on interior points and reflects specularly on boundary components not contained in S. When the potential function is constant, this reduces to a pure billiard system, that is, to geodesic flow with specular collisions at boundary points.

1.2.2 The return map and its canonical invariant measure

Define the *return time* to be the measurable function $\tau : W_r \to (0, \infty]$ such that

$$\tau(p, v) := \inf\{t > 0 : \Phi_t(p, v) \in S\}$$

Under the assumption above, τ is finite for μ_r-almost every (p, v). This is a consequence of Poincaré's lemma in ergodic theory. Thus, it makes sense to define a measurable transformation $R : W_r \to W_r$ called the *first return map* as follows. Now let $R = C \circ \Phi_\tau$. In words, the particle enters at (p, v), follows the Hamilton flow until the first return to S, whereupon it experiences specular collision. This final collision directs the particle back into X. Note that energy is invariant under R, so that the final state is in W_r. The form Ω_r on W_r is invariant under R, so this transformation preserves the probability measure μ_r.

The map R is often much more than measurable. In many cases, W_r has has an open, dense set of full μ_r-measure on which R is well-defined (τ is finite) and smooth. We will assume as much going forward. See [6] for an elaboration of this point. However, R is rarely smooth on all of W_r even when S is a smooth manifold and there can be points in W_r associated to trapped trajectories for which which τ in infinite. Such "bad" points constitute a set of measure zero.

Let us be more clear about the R-invariant volume form Ω_r. Recall the measurable orthonormal frame Let $e_1, ..., e_{n-1}, \mathbf{n}$ on S. Denote the upper half sphere of radius 1 of dimension $n - 1$ by

$$\mathbb{H}_1 = \mathbb{H}_1^{n-1} := \{u \in \mathbb{R}^n : |u| = 1 \text{ and } u_n > 0\} \tag{1.5}$$

12

and denote its Riemannian volume form by ω_k^{n-1} (where k is for "kinetic") or just ω_k where no confusion arises. We also denote by ω_s, the Riemannian volume form on S (here "s" stands for spatial).

In these coordinates, write

$$v = v_1 e_1(p) + ... + v_n e_n(p)$$

$$h(v) = \frac{1}{||v||}(v_1, ..., v_n)$$

And define the map $G_r : W_r \rightarrow S \times \mathbb{H}_1$ by

$$G_r(p, v) = (p, h(v)) \tag{1.6}$$

Note that this map is not surjective except in the case of constant potential on S. To wit, given a in the interior of the range of V, there are points $p \in S$ such that $V(p) > a$, so that no point (p, v) is in W_r. Let χ_r be the characteristic function of the set

$$S_r = \{p \in S : V(p) < \frac{1}{2}r^2\} \tag{1.7}$$

G_r restricts to a diffeomorphism on an open dense set of full μ_r-measure.

Lemma 1.0.1. *The pushforward of the R-invariant measure Ω_r on W_r is, up to a non-zero constant, the $(2n - 2)$-form*

$$G_{r*}(\Omega_r) = \chi_r(p)u_n\omega_s \wedge \omega_k^{n-1} = \chi_r(p)\cos\phi\omega_s \wedge \omega_k^{n-1}$$

for almost every (p, u) relative to the normalized volume measure on $S \times \mathbb{H}_1$.

This lemma generalizes to our present setting (of Riemannian manifolds with non-trivial boundary and potentials) a well-known fact regarding the form of the

invariant measure for 2-dimensional Euclidian billiard maps. For a proof in this standard 2-dimensional setting see, for example, [6]. We suspect that the lemma is known to the experts in the context of classical statistical mechanics. Because of this, and due to time constraints, we decided not to include our proof here, which would require a somewhat long detour into Riemannian geometry. (Even in the standard 2-dimensional case without potentials the proof, such as the one given in [6], while elementary, is not entirely trivial). On the other hand, since we have not found a reference for the lemma in the literature, we plan to add an abbreviated account of its proof in a future paper.

The simple remark that the invariant measure of the billiard map for 2-dimensional billiard tables corresponds to the area measure on the 2-sphere (see figure 1.6) is not widely known. To the best of our knowledge it was first noted in [1].

1.2.3   Interface with Measured Fiber Bundles

Now, let us recognize the elements of the measured fibration framework in the setting of mechanics. We now suppose that S decomposes as a Riemanninan product $S = S^x \times S^y$ of manifolds of dimensions m_x and m_y so that $m_x + m_y = n - 1$. As before, let $e_1, ..., e_{n-1}$ be a measurable orthonormal frame on S with $e_n = \mathbf{n}$, but now assume it is adapted to the product $S^x \times S^y$, so that $e_1, ..., e_{m_x}$ are tangent to S^x and $e'_1 := e_{m_x+1}, ..., e'_{m_y} := e_{m_x+m_y}$ are tangent to S^y. Under the natural identification of TS with $TS^x \oplus TS^y$, we can think of each e_i (resp. e'_j) as vector fields on S or on S^x (resp. S^y).

14

This decomposition will encode our choice of hidden variables (the e_i) and observable variables (the e'_j and e_n). For all entry states

$$W := \{(p, v) : p \in S, E(p, v) > 0, \text{ and } \langle v, \mathbf{n} \rangle > 0\} \tag{1.8}$$

consider the map from W into the upper half space of $\mathbb{R}^n$ given by

$$G(p, v) = (p, r(p, v)h(v)) = (p, \dot{x}_1, ..., \dot{x}_{m_x}, \dot{y}_1, ..., \dot{y}_{m_y}, \dot{z}) \tag{1.9}$$

which, is a well-defined diffeomorphism on the open, dense set of full measure carrying the adapted frame. Then we identify U as the image of G

$$U := G(W)$$

$$F := G^{-1} \circ R \circ G$$

$$\pi(p, \dot{x}_1, ..., \dot{x}_{m_x}, \dot{y}_1, ..., \dot{y}_{m_y}, \dot{z}) := (\dot{y}_1, ..., \dot{y}_{m_y}, \dot{z})$$

Observe that we can also express G in spherical coordinates on the upper half space of $\mathbb{R}^n$ as

$$G(p, v) = (p, h(v), r(p, v)) = (G_r(p, v), r(p, v)) \tag{1.10}$$

For notational ease, denote

$$\dot{\mathbf{x}} := (\dot{x}_1 ... \dot{x}_{m_x}) \in \mathbb{R}^{m_x}$$

$$\dot{\mathbf{x}}^2 := \dot{\mathbf{x}} \cdot \dot{\mathbf{x}}$$

$$\dot{\mathbf{y}} := (\dot{y}_1 ... \dot{y}_{m_y}) \in \mathbb{R}^{m_y}$$

$$\dot{\mathbf{y}}^2 := \dot{\mathbf{y}} \cdot \dot{\mathbf{y}}$$

$$r^2 := \dot{\mathbf{x}} \cdot \dot{\mathbf{x}} + \dot{\mathbf{y}} \cdot \dot{\mathbf{y}} + \dot{z} \cdot \dot{z}$$

So, given $b = (\dot{\mathbf{y}}, \dot{z}) \in B = \pi(U)$, the fiber over b is somewhat complicated:

$$\pi^{-1}(\dot{\mathbf{y}}, \dot{z}) = \{(p, \dot{\mathbf{x}}) \in S \times \mathbb{R}^{m_x} : \dot{\mathbf{x}} \cdot \dot{\mathbf{x}} + \dot{\mathbf{y}} \cdot \dot{\mathbf{y}} + \dot{z} \cdot \dot{z} > V(p)\} \qquad (1.11)$$

However, we may use the much simpler fiber $S \times \mathbb{R}^{m_x}$ with the restriction that the probability kernel η_b be supported on the set above. As we said earlier, we may use the characteristic function χ_r for this purpose.

Theorem 1.1. *Let* $g(x) = \frac{1}{\sqrt{2\pi\sigma^2}} e^{-x^2/2\sigma^2}$ *and* $m(x) = \frac{1}{\sigma^2} x e^{-x^2/2\sigma^2}$. *Suppose the probability kernel* η *is given by*

$$\eta_{(\dot{\mathbf{y}}, \dot{z})} = (c_\eta \chi_r(p) d\omega_s) \left(\Pi_{i=1}^{m_x} g(\dot{x}_i) d\dot{x}_i \right)$$

Then the measure

$$\nu = \left(\Pi_{j=1}^{m_y} g(\dot{y}_j) d\dot{y}_j \right) (m(\dot{z}) d\dot{z})$$

on B *is* P_η*-stationary, where* c *normalizes. Changing to spherical coordinates on* B *and denoting the radius and polar angle by* s *and* φ *respectively, we obtain*

$$\nu = \left(c_\varphi \cos \varphi d\omega_k^{m_y} \right) \left(c_s s^{m_y+1} e^{-s^2/2\sigma^2} ds \right)$$

where the constants normalize.

As we shall see in 4, the proof involved the recognition that the measure $\nu \circ \eta$ expressed in spherical coordinates on U is induced by the wedge of the form in lemma 1.0.1 and a smooth 1-form on $\rho(r) dr$. Since this form is invariant under the dynamical map F, it induces an invariant measure on U which projects to ν. Then by lemma 2.0.1, ν is stationary.

16

Recall that m_y does not count the distinguished normal variable, so that we have

$$m_y + 1 = n - m_x$$

Recall that, after normalization, $x^{d-1}e^{-x^2/2\sigma^2}$ is the Maxwell-Boltzmann distribution in dimension d with parameter σ. It is known to probabilists as the chi distribution with d degrees of freedom with parameter σ, and we hereafter denote $\chi_d(\sigma)$.

In the case $V \equiv 0$ on S (as in the gas-surface interaction model with moving parts), χ_r is supported on all of S for all $r > 0$ (a particle with positive energy can enter at any point of S). So we may drop all the χ_r above and record the following corollary in words.

Corollary 1.1.1. *Suppose V is constant on S. Then if the spatial variables are chosen according to the uniform distribution on their domain and the hidden kinetic variables are each chosen according to the Gaussian distribution with mean 0 and variance σ^2, then the measure distributed according the Maxwell-Boltzmann distribution of dimension $m_y + 2$ with parameter σ on (macroscopic) speed, and according to $\cos \varphi \omega_k^{m_y}$ (Knudsen's Cosine Law) on (macroscopic) angle of reflection is stationary.*

1.2.4   Examples

We briefly give a number of examples to illustrate the general type of system introduced in the previous subsection.
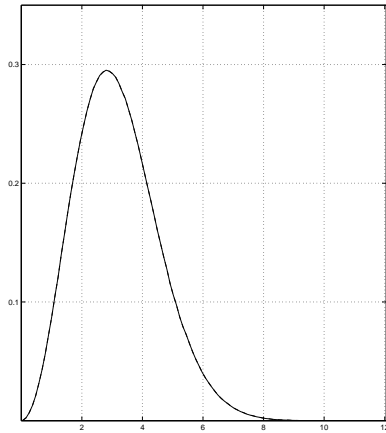
Figure 1.4. 3-dimensional Maxwell-Boltzmann distribution with $\sigma = 2$

First, we revisit the example given earlier. Figure 1.5 demonstrates the macroscopic/microscopic interface. The solid black line at the bottom of the figure may be thought to represent part of the surface of a two-dimensional container in which we have placed some "billiard gas." The surface appears flat at the macroscopic scale, but by zooming in near the point of impact, we see a "microscopic" curved contour. Note our microstructure is slightly more general now than in the prior instance of this example. This microstructure causes the particle to scatter at angle different than specular reflection.
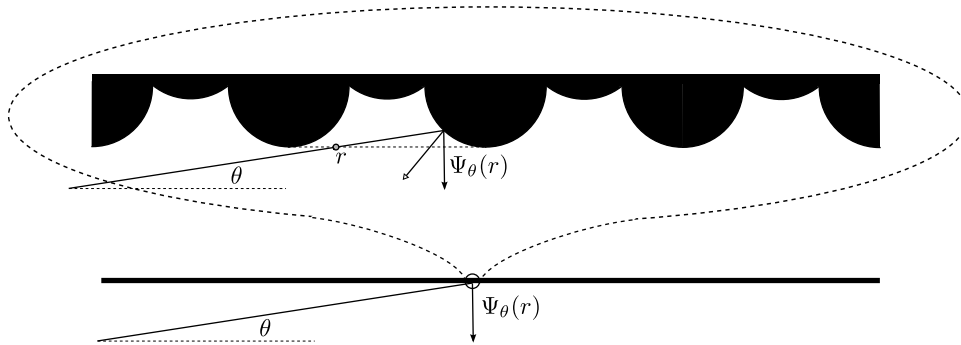
Figure 1.5. Surface with a microscopic periodic texture

For consistency with the analysis of this example in [1], we denote the point and angle of incidence by $r \in [0, 1]$ and $\theta \in [0, \pi]$, though in later chapters, the same quantities will be denoted $p_y \in [-W, W]$ and $\varphi \in [-\pi/2, \pi/2]$. The angle of reflection is denoted by $\Psi_\theta(r)$ and potential is constant.

Now, regard r as a random variable with the uniform distribution on the interval (thus r is a hidden variable) and θ as an observable variable. This leads to a one dimensional random dynamical system $\theta \mapsto \Psi_\theta(r)$ in the space of angles $V = [0, \pi]$. We note that the particle can not change speed in this case (elastic collisions) so that speed is fixed by the initial value of the energy function.

$$ M = \qquad \stackrel{\cong}{\Longrightarrow} $$

$$ \pi \downarrow $$

$$ V = [0, \pi] $$
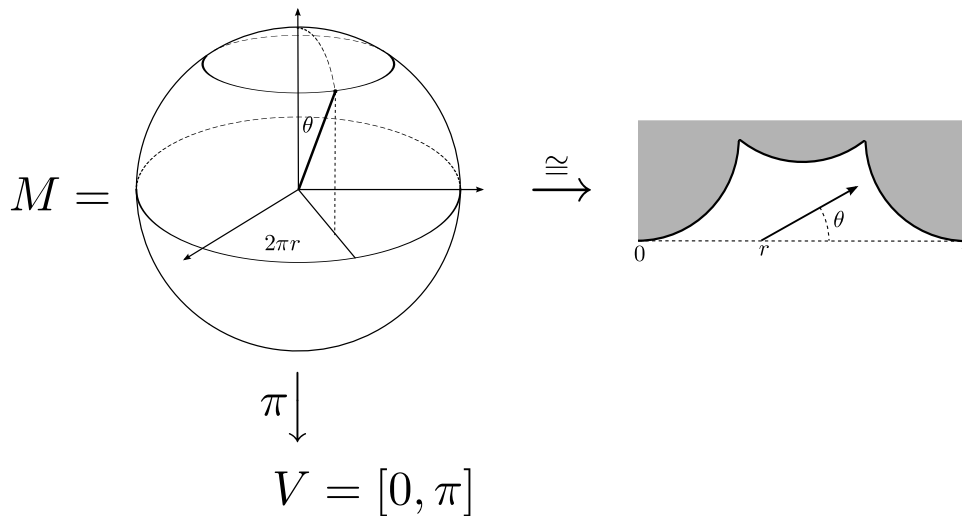
Figure 1.6. The measured fiber bundle for the example above. The measures on fibers are obtained by disintegration of the area measure on the 2-sphere

It is interesting to observe that the deterministic state of the system (at a moment of entry or exit from one billiard cell) can in this case be represented by a point on the standard unit 2-sphere with spherical coordinates θ and $2\pi r$. See figure 1.6 in which

19

π denotes the projection map onto observable states. The right hand side of figure 1.6 represents a billiard cell of the periodic contour. Representing the state space (of deterministic states) as a 2-sphere is both natural and convenient for systems of this kind since the invariant probability measure under the return map coincides with the normalized standard area measure.

The Markov operator can be described in this case as follows. If ν is the stationary measure (in this case $d\nu(\theta) = \frac{1}{2}\sin\theta d\theta$) and $f \in L^{\infty}(V, \nu)$, then

$$(Pf)(\theta) = \int_0^{\pi} f(\Psi_\theta(r))dr \qquad (1.12)$$

Figure 1.7 shows a few steps in the evolution of an intial probability distribution of angles.
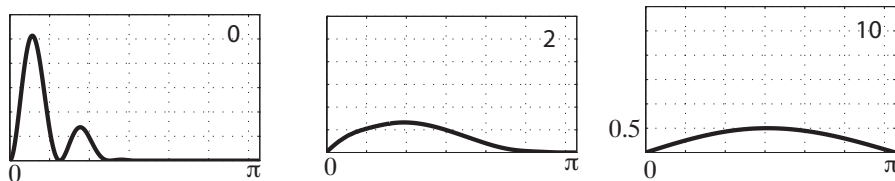
Figure 1.7. The leftmost graph gives an arbitrary initial distribution of angles, defines as a probability density with respect to Lebesgue measure on the interval. After 2 collisions, (i.e. 2 applications of the operator P) the density has evolved as shown in the middle plot. After 10 collisions, we have the plot on the right, which seems to well approximate the stationary measure $\frac{1}{2}\sin\theta d\theta$

As a variant, consider figure 1.8. Much of the analysis for the prior example would also apply to this case except that the entry/exit boundary has two connected components.

20
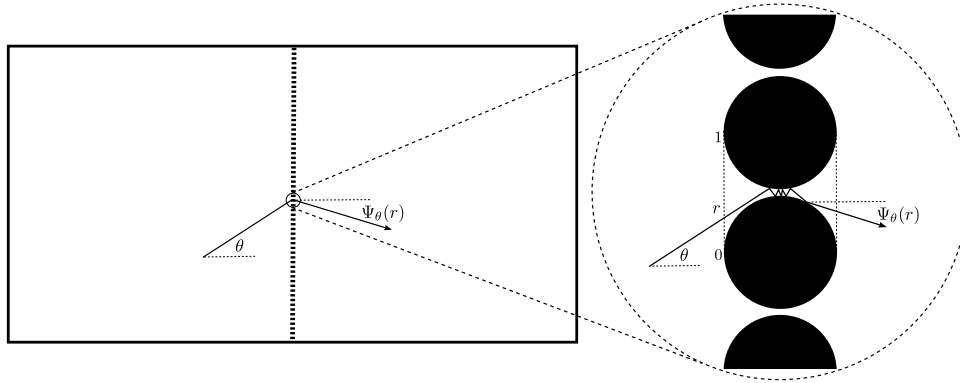
Figure 1.8. The box on the left-hand side represents a chamber separated by a "billiard membrane." Zooming in on a small part of the membrane shows a linear chain of hard discs. A billiard molecule that collides with the membrance can scatter back into the same half chamber of pass through to the other side.

The example depicted in figure 1.9 is similar to the previous ones in spirit, but has the added feature that there are additional masses that can move freely within a short range of the surface of the container. Once the bound particle reaches the end of its limit of free motion, it bounces back elastically. This is a version of the model we explore in detail later in the thesis. In this case, the speed of the gas particle (labeled m_2 in this image) does not necessarily stay the same after an impact event.

A primary result of this thesis in the determination of the stationary distribution for this model. It is natural to assume that that the intial positions of both particles are distributed uniformly at random on their domains and that the intial velocity of the bound particle is distributed normally with mean 0 and variance $\tilde{\sigma}^2$. Under these assumptions, we will prove that the stationary distribution for the speed of the gas particle is the famous Maxwell-Boltzmann distribution (with parameter determined
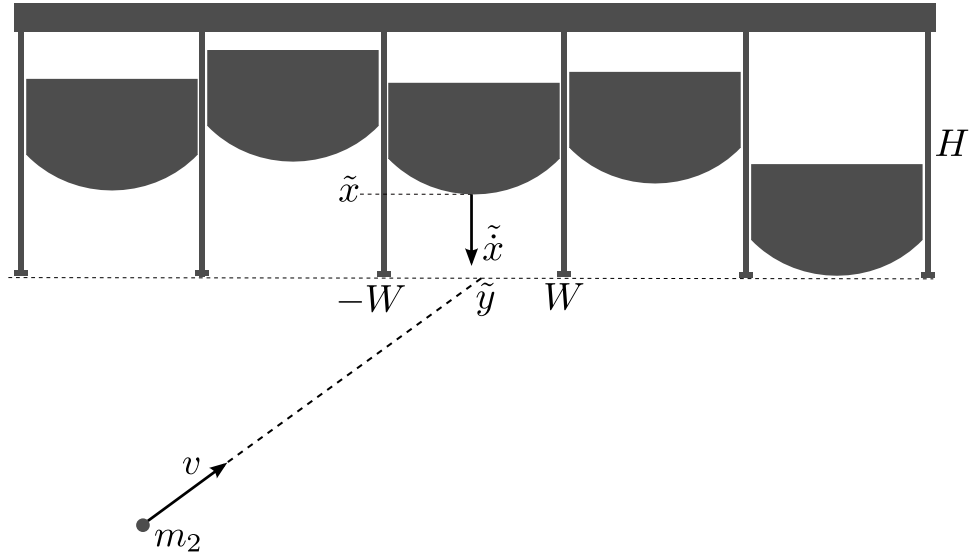
Figure 1.9. Microstructure with moving parts. In this case, the scattering surface contains moving parts whose initial kinetic state is unknown and therefore chosen according to some random distribution.

by $\tilde{\sigma}^2$), while the stationary distribution for angle of reflection continues to follow the $\frac{1}{2}\sin\theta d\theta$ law encountered in the non-moving parts models above.

Consider now the system depicted in figure 1.10. This is essentially also a case where the norm of the velocity (properly interpreted) stays constant after a collision event, although the cosine law has to be described in dimension 3 since the configuration manifold in 3-dimensional. It is assume here that the potential function is constant. Let us first described the configuration manifold (a Riemannian manifold with boundary).

Let l by the (fixed) length of the arm connecting the two (for simplicity point) masses comprising the molecule and write $m = m_1 + m_2$ for the total mass. The x-axis is fixed parallel to the surface and the y-axis perpendicular to it poiting up
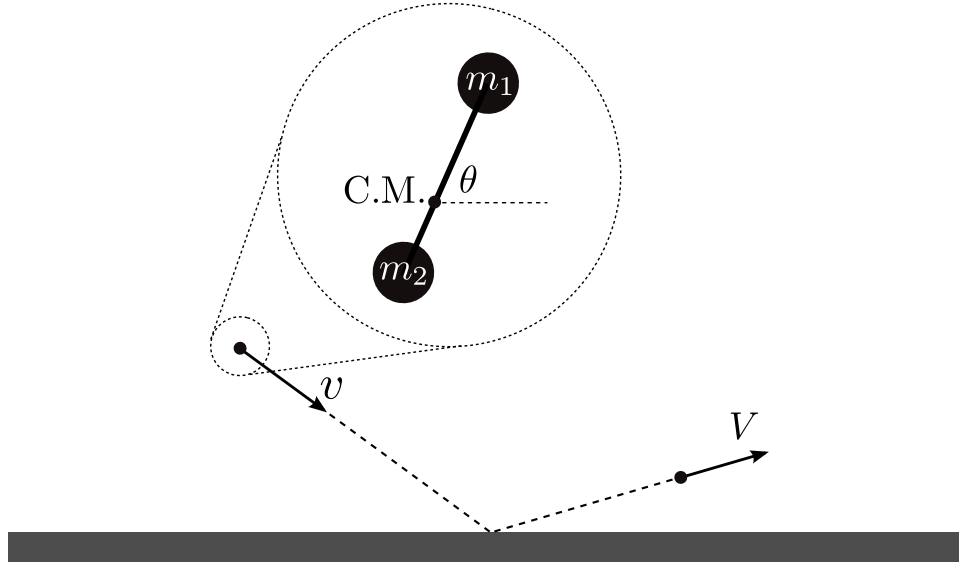
Figure 1.10. A "diatomic billiard molecule" bouncing off a flat surface in dimension 2

and let (x, y) represent the coordinate of the center of mass. Then the configuration manifold is given by

$$M = \{([\theta], x, y) : \min\{y - \frac{m_2}{m}l\sin\theta, y + \frac{m_1}{m}l\sin\theta\} \geq 0\} \qquad (1.13)$$

Here $[\theta]$ represents an element in $\mathbb{R}/2\pi\mathbb{Z}$. M is represented in figure 1.11 and a (θ, y) cross section of M is shown in figure 1.12. To complete the description of the configuration manifold, we need to specify the Riemannian metric. In order for collisions to correspond to specular reflection, the Riemannian metric should correspond to the kinetic energy function. By introducing the scaled angle coordinate

$$z := \frac{\sqrt{m_1 m_2}}{m}l\theta \qquad (1.14)$$

23
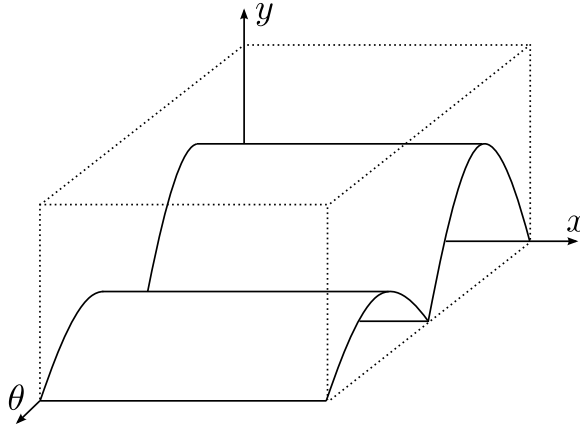
Figure 1.11. The configuration manifold for the diatomic billiard molecule corresponds to the subset of the coordinate (θ, x, y)-space consisting of points that lie above the curved roofs. The roofs comprise the reflecting boundary and the back and front planes parallel to the (x, y)-coordinate plane are periodic boundaries. The manifold is invariant under translations in the x-direction (there are no boundaries parallel to the (y, θ)-plane. The billiard particle enters the region of interaction through the plane $y = c$ lying above the roofs.

it is an elementary calculation to see that the kinetic energy, as a function of the coordinates $(x, y, z, \dot{x}, \dot{y}, \dot{z})$ on the tangent bundle of M, takes the form

$$E(x, y, z, \dot{x}, \dot{y}, \dot{z}) = \frac{1}{2}m(\dot{x}^2 + \dot{y}^2 + \dot{z}^2) \qquad (1.15)$$

which corresponds to the standard Euclidean metric in regions of $\mathbb{R}^3$. So, in terms of these new coordinates, collisions are described by ordinary specular reflection on the boundary of M. (We are assuming here that the surface is perfectly smooth the the physical sense, i.e. there is no tangential transfer of momentum between the particles and the surface).

By restricting attention to a cross section ($x = $ constant), this 3-dimensional system can be reduced to a 2-dimensional system that is essentially like the one of
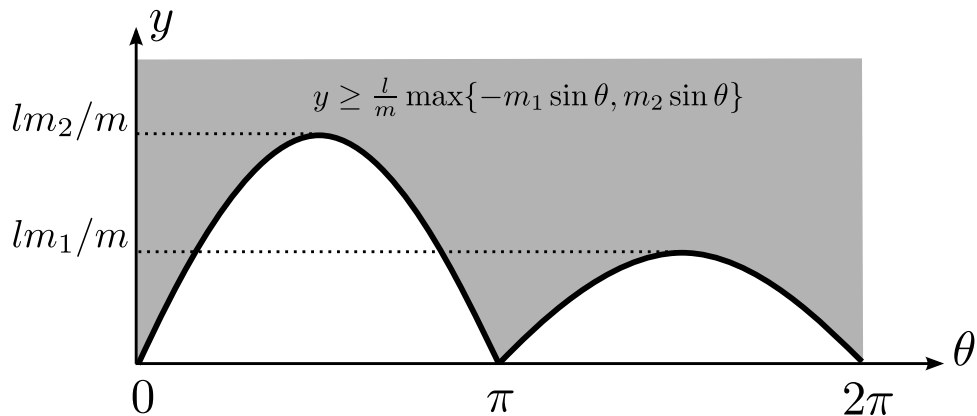
Figure 1.12. A cross section of figure 1.11

figure 1.5, with z (representing the hidden variable) playing the role of r. Thus, we obtain a random process under the assumption that the angle of rotation is entirely unknown at any given moment. This example bring attention to the following point. The surface description should be understood in each case as representing the particle-surface interaction and not some intrinsic geometry of the material surface by itself.

This point is further illustrated by considering example of figure 1.5, where the gas particle is given a positive radius. By "thickening" the surface in the amount of the radius of the particle, we may return to assuming the particle is a point mass, behaving as though the surface has an effective shape that is different from its actual shape.

One last example is shown in figure 1.13. We regard this as a one-dimensional system. The region of interaction is the interval $[0, l]$, where $l > 0$. Using scaled coordinates

$$x = \sqrt{\frac{m_1}{m}} \left(x_1 - \frac{l}{2} \right), y = \sqrt{\frac{m_1}{m}} \left(x_2 - \frac{l}{2} \right) \tag{1.16}$$

25
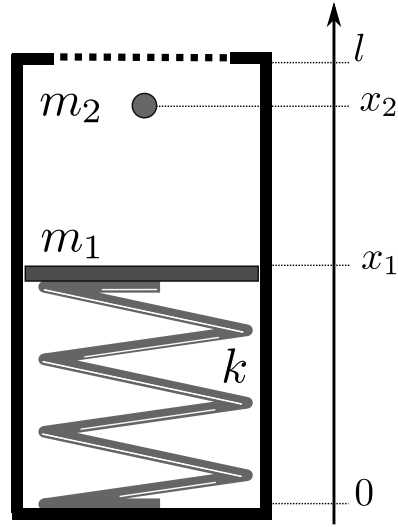
Figure 1.13. A 1-dimensional spring-mass system. We assume that at the moment the mass m_1 enters the region of interaction, the kinetic state of m_2 is chosen at random according to a fixed probability distribution

for the positions of the masses m_1 and m_2 respectively,, the Lagrangian for the system with the potential of a linear spring is given by

$$L(x, y, \dot{x}, \dot{y}) = \frac{m}{2}(\dot{x}^2 + \dot{y}^2) - \frac{k}{2}x^2 \tag{1.17}$$

which is defined on the tangent space of the configuration space shown in 1.14

It is easily shown that the equations of motion are solved (between collisions with the boundary of the boundary of the configuration manifold) by the functions to t

$$x(t) = x_0 \cos\left(\sqrt{\frac{k}{m}}t\right) + \dot{x}_0\sqrt{\frac{m}{k}}\sin\left(\sqrt{\frac{k}{m}}t\right) \tag{1.18}$$

$$y(t) = \dot{y}_0 t + y_0 \tag{1.19}$$

The random process is now obtained from the deterministic system as follows. For any given value $v \in (0, \infty)$ of the velocity of m_2 (where $v > 0$ indicates that
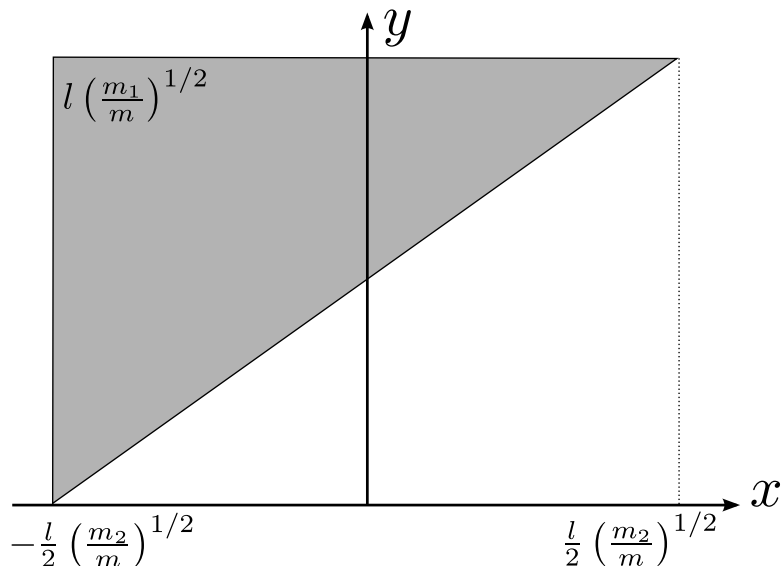
Figure 1.14. Configuration manifold for the 1-dimensional spring-mass system. Points on the diagonal boundary line represent configurations in which the two masses are in contact. The vertical boundary component consists of configurations in which the bound mass bumps against the floor at level 0. The horizontal component at the top represents the entry/exit boundary component. We have adjusted the scales so that the kinetic energy becomes the standard Euclidean metric in $\mathbb{R}^2$.

the free particle is approaching the spring-mass system and we are using the rescaled coordinates), choose a random point on the top horizontal boundary segment of the triangle of figure 1.14 and a random velocity w for the mass m_1 normally distributed with mean 0 and variance σ^2. Now, form the initial 2-dimensional velocity with the latter velocity as the x-component and $-v$ as the y-component. Then trace the trajectory with this initial condition inside the triangle until it re-emerges at the top boundary line. The vertical component of the final velocity is the new state of the Markov chain.
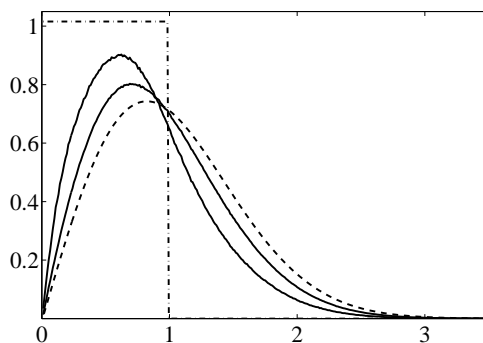
Figure 1.15. The square shown in the dash-dot lines is the graph of an initial probability density ρ_0. The taller of the two graphs in solid line describes the first iterate of ρ_0 under the Markov operator for the above spring-mass system. The shorter graph in solid line represents the second iterate, and the dashed line is the graph of the stationary density, $\rho_\infty(u) = \frac{u}{\sigma_1^2} \exp(-u^2/2\sigma_1^2)$, where u is the rescaled velocity of the free particle and σ_1 is the rescaled variance of the bound particle velocity. In the original (non-rescaled) variables, this corresponds to $\rho_\infty(v) = \frac{m_2 v}{\tau} \exp(-m_2 v^2/2\tau)$ where the parameters used are: spring constant $k = 1$, bound particle mass $m_1 = 2$, free particle mass $m_2 = 1$ ($m = m_1 + m_2$) and the "temperature" $\tau = m_1\sigma^2$, for $\sigma = 1$

1.3   Synopsis of Main Results

The gas-surface interaction model with moving part shown in figure 1.9 is the central focus of most of the remainder of this thesis. As noted previously, this sort of model was first considered by Feres and Yablonsky [7] and further developed in [1,8]. The addition of moving parts is new in this work and we describe it carefully in chapter 3.

The addition of the moving parts allows both speed and angle of the free particle to change during an impact with the surface of its container, but it also adds complication to the analysis used in the prior papers. The need to handle random

choices for multiple quantities, and in particular for kinetic quantities, motivated us to define the measured fibration framework we will explore in chapter 2. We believe this framework will provide a fruitful language for future exploration of the types of models outlined above.

The first step in the analysis of this Markov chain is identifying the stationary distribution. In chapter 4, we will finish the proof begun above that, in the case of uniform distribution on position and Gaussian distribution on velocity, the Maxwell-Boltzmann distribution is stationary for the speed of the free particle and cosine of the polar angle times the surface area measure on the upper half sphere in stationary for the angle of reflection of the free particle. We will also show that the Markov chain is self-adjoint under a symmetry assumption on the shape of the bound particle.

In addition to the random distribution of the hidden variables, there are several physical parameters within the moving parts model - primarily bound particle shape and ratio of masses of the particles. In the Gaussian model referenced above, the physical parameters make no difference to the stationary distribution, though they do appear to impact spectral properties (as will be seen in chapter 5). However, we will see that under other ways of choosing the hidden variables, the physical parameters do impact stationary distribution. In chapter 5, we will present simulation studies performed under these regimes.

At the end of chapter 4, we will approach the non-Gaussian case by approximating our Markov operator by a differential operator in the limit as the ratio of masses increases. We will show that this approximating operator can be written in the form

of a Sturm-Liouville equation. We are hopeful that we can use the well understood spectral properties of such operators to understand the spectrum of our Markov operator. This approach is key in [1] and we believe it will work in the moving parts model now that the stationary distribution has been established. It is interesting to note that, even in the non-Gaussian situation, this approach suggests that the Maxwell-Boltzmann distritbution should be stationary as the ratio of masses goes to infinity, as the numerical evidence suggests.

1.4   Context

The broad perspective in this work in to create general state Markov chains from deterministic systems. So, where does this work fit in the broader mathematical scope?

Some of the central problems in the theory of Markov chains are establishing various forms of ergodicity, describing stationary distributions, obtaining information about rates of convergence to equilibrium (decay of correlations, mixing times), establishing spectral properties, etc. These are of great practical interest. For example, applications of Markov Chain Monte Carlo methods in statistics depend on having some understanding of convergence times. In statistical physics (one of the key sources of MCMC problems historically), rates of decay of correlation and spectral information are needed to obtain transport quantities (diffusion constants, conductivities, etc) for systems of various kinds.

These problems can be very challenging in the general situation. Thus, it is of practical interest to begin from probabilistic systems that are naturally and canonically related to deterministic systems. Then the statistical behavior of the probabilistic systems can be analyzed using the known behavior of the determinstic system. This is the case for the Markov models considered in this thesis. Thus, this work potentially draws from many areas of mathematics. Moreover, has been shown that it is sometimes true that a random version of a hard problem can be easier; we hope we might be able to make such a contribution to these venerated fields.

1. Ergodic Theory and Chaotic Dynamics - Conservative mechanical systems with collisions (billiard systems) have long held a place of special interest in the general theory of dynamical systems. Much of the mathematical terminology used in the study of hyperbolic dynamics (chaotic systems, entropy theory, proofs of ergodicity, etc.) was derived over the course of many decades by Sinai, Pesin, Ledrappier and Young, Chernov, and many others. The intent was to prove that simple hard-spheres models of gas are ergodic. This work tends to be extremely technical, in part because the goal was to derive statistical behavior directly from the purely deterministic dynamics. Randomization of the problems might prove a useful technique.

2. Random Dynamical Systems - There has been much activity in the past few decades to extend the classical theory of dynamical systems to random dynamical systems. An early exponent of this is Y. Kiefer. See also Ludwig Arnold.

The perspective of random dynamical systems is also present in such topics as stochastic iterated function systems (M. Barnsley). Our billiard models provide a particularly rich class of systems that can be used to inform further development of the theory of random dynamics. (Random Lyapunov exponents, random entropy, etc.)

3. Boltzmann Equations - The theory of Boltzmann equations seeks to provide a proper modern foundation for the kinetic theory of gases. This topic dates to Boltzmann's work and is of great current interest, as attested by the Field's medal awarded to Cedric Villani in 2010 for his work in this area. As noted in [9], the theory involves the choice of boundary operators. The Markov operators described in this thesis can be regarded as providing these boundary operators from an underlying physical mechanism.

4. Applications outside of mathematics - This works has been partly motivated by the problem of determining diffusion coefficients for gases under the so-called Knudsen regime of long mean free paths. (Collaboration with Grigoriy Yablonksy.) For such gases, collisions between gas molecules are infrequent compared to collisions with the surface of the container. In this regime (which requires low pressures but not quite vacuum conditions), obtaining good estimates for diffusion constants is of considerable interest in certain areas of chemical engineering. An example is a new type of chemical reactor (referred to as TAP reactors) based on the idea that one can obtain fine information about

chemical reaction mechanisms for certain catalytic systems in the presence of controlled diffusion by carefully studying the system in the absence of catalysts. In this case, only diffusion occurs; one then studys the changes in gas transport (diffusion properties, exit times for gas outflow) due to the introduction of the catalyst. In these studies, a precise determination of diffusion constants is important. Simple collision models of the type studied in this thesis provide a way to understand these issues starting from a more fundamental and principled basis.

1.5 The plan

In chapter 2, we describe the measured fibration language in some detail and catalogue some useful facts. At this level of generality, much more can be said. Then, in chapter 3, we describe the specific gas-surface interaction model with moving parts. Then, in chapter 4, we will present our proof that the stationary distribution for the Gaussian version of this model is Maxwell-Boltzmann, and we show that this version of the model is self-adjoint. We will also consider a non-Gaussian version in a the limit as the ratio of particle mass $\epsilon \to \infty$. In chapter 5, we will present the results of our simulation studies, including estimates for spectral gap in the Gaussian version and plots of the rather surprising stationary distributions that arise from some non-Gaussian versions.

2. Measured Fibrations

In this chapter, we will describe the measured fibration framework in detail and prove some basic facts which we will later use to analyze our specific models.

2.1 Definition

We first briefly recall a few elements of measure theory. Given a measure space U, let $\mathscr{P}(U)$ denote the space of probability measures on U. Though measures are often first encountered as objects that operate on subsets of U and provide a notion of size, they are more generally viewed as objects that operate on measurable functions $f : U \to \mathbb{R}$ by integration $\mu(f) = \int_U f(u)d\mu(u)$. We adopt this second viewpoint and note that the first can be recovered by integrating the characteristic function $\mathbb{1}_A$ for a subset A of interest.

Recall the notion of the pushforward of a measure. Let U and V be measure spaces, $\mu \in \mathscr{P}(U)$, and $F : U \to V$ be a measurable map. Then the pushforward $F_*\mu$ acts on measurable functions $f : V \to \mathbb{R}$ by

$$(F_*\mu)(f) := \int_U (f \circ F)(u)d\mu(u) = \mu(f \circ F) \tag{2.1}$$

Letting $f = \chi_A$, we obtain the familiar $(F_*\mu)(A) = \mu(F^{-1}(A))$ for $A \subset V$ measurable.

Note that $G_* \circ F_* = (G \circ F)_*$ since for $G : V \to W$ and $f : W \to \mathbb{R}$

$$(G_*(F_*\mu))(f) = (F_*\mu)(f \circ G) = \mu[(f \circ G) \circ F] = \mu[f \circ (G \circ F)] = ((G \circ F)_*\mu)(f)$$

We say μ is $\underline{F\text{-invariant}}$ if $F : U \to U$ and $F_*\mu = \mu$

This leads us to describe the $\underline{\text{measured fibration}}$ framework. Let U and B be measure spaces and $\pi : U \to B$ a surjective measurable map and $F : U \to U$ an invertible measurable map. For $b \in B$, we call $\pi^{-1}(b)$ the $\underline{\text{fiber over } b}$ and call b the $\underline{\text{base}}$. Fix a family $\eta = (\eta_b)_{b \in B}$ of probability measures on the fibers called a $\underline{\text{probability kernel}}$.

Given $\nu \in \mathscr{P}(B)$, define $(\nu \circ \eta) \in \mathscr{P}(U)$ by

$$(\nu \circ \eta)(f) := \int_B \int_{u \in \pi^{-1}(b)} f(u) d\eta_b(u) d\nu(b). \tag{2.2}$$

This says "average f over each fiber using η then average over the set of fibers using ν". This defines a measure on U under the condition on η that the function on B produced by the inner integration is measurable; all our examples satisfy this condition.

Proposition 2.0.1. $\pi_*(\nu \circ \eta) = \nu$

Proof.

$$\pi_*(\nu \circ \eta)(f) = (\nu \circ \eta)(f \circ \pi)$$

$$= \int_B \int_{u \in \pi^{-1}(b)} f(\pi(u)) d\eta_b(u) d\nu(b)$$

$$= \int_B f(b) \left(\int_{u \in \pi^{-1}(b)} d\eta_b(u) \right) d\nu(b)$$

η_b is a probability measure

$$= \int_B f(b) d\nu(b)$$

$$= \nu(f)$$

$\square$

Given $\mu \in \mathscr{P}(U)$, define a <u>disintegration of μ</u> to be a probability kernel η_μ such that $\mu = \pi_* \mu \circ \eta$.

Define the Markov operator P_η on $\mathscr{P}(B)$ by

$$P_\eta : \nu \mapsto (\pi \circ F)_*(\nu \circ \eta) \tag{2.3}$$

So, P_η provides the evolution of our random system. We will typically follow the convention that P_η acts on measures from the right. The action on functions is expressed by

$$(\nu P_\eta)(f) = (\nu \circ \eta)(f \circ \pi \circ F) = \int_B \int_{u \in \pi^{-1}(b)} f((\pi \circ F)(u)) d\eta_b(u) d\nu(b) \tag{2.4}$$

Then define

$$(P_\eta f)(b) = \int_{u \in \pi^{-1}(b)} f((\pi \circ F)(u)) d\eta_b(u) \tag{2.5}$$

37

So that

$$(\nu P_\eta)(f) = \nu(P_\eta f) \qquad\qquad (2.6)$$

$$
\begin{array}{ccc}
U & \xrightarrow{F} & U \\
\pi\downarrow & & \downarrow\pi \\
B & \xrightarrow[\text{random map}]{} & B
\end{array}
\qquad \nu \mapsto \nu P := (\pi \circ F)_* \nu \circ \eta
$$

Figure 2.1. A Measured Fibration

We say ν is P_η <u>stationary</u> if $\nu P_\eta = \nu$.

Lemma 2.0.1. .

1. If $\mu = \nu \circ \eta$ is F-invariant, then ν is P_η stationary.

2. If $\mu \in \mathscr{P}(U)$ is F-invariant and η_μ is a disintegration of μ, then $\pi_* \mu$ is P_{η_μ}-stationary.

Proof.

$$(\nu P_\eta)(f) = \int_B \int_{u \in \pi^{-1}(b)} f((\pi \circ F)(u)) d\eta_b(u) d\nu(b)$$

$$= \int_U f((\pi \circ F)(u)) d\mu(u)$$

let $v = F(U)$

$$= \int_U f(\pi(v) d\mu(F^{-1}(v))$$

μ is F-invariant

$$= \int_U f(\pi(v) d\mu(v)$$

$$= \int_B \int_{v \in \pi^{-1}(b)} f(\pi(v)) d\eta_b(u) d\nu(b)$$

$$= \int_B f(b) \left(\int_{v \in \pi^{-1}(b)} d\eta_b(u) \right) d\nu(b)$$

$$= \int_B f(b) d\nu(b)$$

$$= \nu(f)$$

The second part follows from the first with $\nu = \pi_* \mu$. $\qquad\square$

2.2 $L^2(B, \nu)$

We use $P_{\eta,F}$ to explicitly name the map F when needed. Beyond this point, we assume that $\mu = \nu \circ \eta$ is F-invariant so that ν is $P_{\eta,F}$-stationary. Consider the Hilbert space $\mathscr{H} = L^2(B, \nu)$ with its natural inner product and norm

$$\langle f, g \rangle_\nu := \nu(f\bar{g}) = \int_B f(b)\bar{g}(b)d\nu(b) \tag{2.7}$$

$$||f||_\nu^2 := \langle f, f \rangle_\nu = \int_B |f(b)|^2 d\nu(b) \tag{2.8}$$

39

Proposition 2.0.2. *If $\mu = \nu \circ \eta$ is F-invariant, then $P_{\eta,F}$ is a bounded linear operator of norm 1 on $L^2(B, \nu)$*

Proof. Linearity follows from properties of the integrals that define $P_{\eta,F}$. To see boundedness, pick $f \in L^2(B, \nu)$ and compute

$$
\begin{aligned}
||P_{\eta,F}f||_\nu^2 &= \int_B |P_{\eta,F}f(b)|^2 \, d\nu(b) \\
&= \int_B \left| \int_{u \in \pi^{-1}(b)} f((\pi \circ F)(u)) d\eta_b(u) \right|^2 d\nu(b) \\
&\leq \int_B \left(\int_{u \in \pi^{-1}(b)} |f((\pi \circ F)(u))| \, d\eta_b(u) \right)^2 d\nu(b) \\
&\leq \int_B \int_{u \in \pi^{-1}(b)} |f((\pi \circ F)(u))|^2 \, d\eta_b(u) d\nu(b) \\
&= \int_U |f((\pi \circ F)(u))|^2 \, d\mu(u)
\end{aligned}
$$

Let $v = F(u)$

$$
= \int_U |f(\pi(v))|^2 \, d\mu(F^{-1}(v))
$$

F-invariance of μ

$$
\begin{aligned}
&= \int_U |f(\pi(v))|^2 \, d\mu(v) \\
&= \int_B \int_{v \in \pi^{-1}(b)} |f(\pi(v))|^2 \, d\eta_b(v) d\nu(b) \\
&= \int_B |f(b)|^2 \left(\int_{v \in \pi^{-1}(b)} d\eta_b(v) \right) d\nu(b) \\
&= \int_B |f(b)|^2 \, d\nu(b) \\
&= ||f||_\nu^2
\end{aligned}
$$

Where the second inequality is an application of Hölder's inequality $||fg||_1 \leq ||f||_2 ||g||_2$.

Interpret these norms as integration along the fiber at b (integration against η_b). Let

f be everything inside the absolute value and g be the constant function 1. Then everything inside the parenthesis is $||fg||_1$. But $||g||_2 = 1$ since η_b is a probability measure, so $||fg||_1^2 \leq ||f||_2^2$ and the next line follows $\qquad\square$

Recall that the <u>adjoint</u> of an operator A on $\mathscr{H}$ is the operator A^* such that

$$\langle f, Ag \rangle = \langle A^*f, g \rangle \text{ for all } f, g \in \mathscr{H} \qquad (2.9)$$

Proposition 2.0.3. *If $\mu = \nu \circ \eta$ is F-invariant, then $\langle f, P_{\eta,F}g \rangle_\nu = \langle P_{\eta,F^{-1}}f, g \rangle_\nu$. In other words $P_{\eta,F}^* = P_{\eta,F^{-1}}$.*

Proof.

$$\langle f, P_{\eta,F}g \rangle_\nu = \int_B f(b) \left(\int_{u \in \pi^{-1}(b)} \bar{g}((\pi \circ F)(u))d\eta_b(u) \right) d\nu(b)$$

$$= \int_B \int_{u \in \pi^{-1}(b)} f(\pi(u))\bar{g}((\pi \circ F)(u))d\eta_b(u)d\nu(b)$$

$$= \int_U f(\pi(u))\bar{g}((\pi \circ F)(u))d\mu(u)$$

Let $v = F(u)$

$$= \int_U f((\pi \circ F^{-1})(v))\bar{g}(\pi(v))d\mu(F^{-1}(v))$$

F-invariance of μ

$$= \int_U f((\pi \circ F^{-1})(v))\bar{g}(\pi(v))d\mu(v)$$

$$= \int_B \int_{v \in \pi^{-1}(b)} f((\pi \circ F^{-1})(v))\bar{g}(\pi(v))d\eta_b(v)d\nu(b)$$

$$= \int_B \bar{g}(b) \left(\int_{v \in \pi^{-1}(b)} f((\pi \circ F^{-1})(v))d\eta_b(v) \right) d\nu(b)$$

$$= \langle P_{\eta,F^{-1}}f, g \rangle_\nu$$

$\qquad\square$

Now, suppose we have a second map $\tilde{J} : U \to U$ such that

1. $\tilde{J}$ is invertible

2. $F \circ \tilde{J} = \tilde{J} \circ F^{-1}$

3. $\tilde{J}$ projects to a map $J : B \to B$; that is $(J \circ \pi) = (\pi \circ \tilde{J})$. Observe that this implies that $\tilde{J}$ is a <u>fibration map</u> - it moves fibers together

$$u_1, u_2 \in \pi^{-1}(b) \implies \exists b' \text{ s.t. } \tilde{J}(u_1), \tilde{J}(u_2) \in \pi^{-1}(b')$$

Then the invertibility of $\tilde{J}$ implies invertibility of J.

4. $\mu = \nu \circ \eta$ is $\tilde{J}$-invariant (as well F-invariant)

5. $\pi \circ \tilde{J}^{-1} = J^{-1} \circ \pi$

J and $\tilde{J}$ are purely deterministic maps which do not depend upon η. Let $Jf := f \circ J$.

Proposition 2.0.4. *If $\mu = \nu \circ \eta$ is F-invariant and $\tilde{J}$ satisfies the conditions above, then $J^* = J^{-1}$.*

Proof. Note that $J_*\nu = \nu$ since

$$J_*\nu = J_*(\pi_*\mu) = (J \circ \pi)_*\mu = (\pi \circ \tilde{J})_*\mu = \pi_*(\tilde{J}_*\mu) = \pi_*\mu = \nu$$

As a consequence, we see

$$\langle f, g \rangle_\nu = \nu(f\overline{g}) = J_*\nu(f\overline{g}) = \nu((f \circ J)\overline{(g \circ J)}) = \langle Jf, Jg \rangle_\nu$$

Thus

$$\langle J^{-1}f, g \rangle_\nu = \langle JJ^{-1}f, Jg \rangle_\nu = \langle f, Jg \rangle_\nu$$

$\square$

Proposition 2.0.5. *Under the conditions above, we have $P^*_{\eta,F} = J^* P_{\eta,F} J$.*

Proof.

$$(P_{\eta,F} Jf)(b) = \int_{u \in \pi^{-1}(b)} Jf((\pi \circ F)(u)) d\eta_b(u)$$

$$= \int_{u \in \pi^{-1}(b)} f((J \circ \pi \circ F)(u)) d\eta_b(u)$$

$$= \int_{u \in \pi^{-1}(b)} f((\pi \circ \tilde{J} \circ F)(u)) d\eta_b(u)$$

$$= \int_{u \in \pi^{-1}(b)} f((\pi \circ F^{-1} \circ \tilde{J})(u)) d\eta_b(u)$$

$$= \int_{u \in \pi^{-1}(b)} (f \circ \pi)((F^{-1} \circ \tilde{J})(u)) d\eta_b(u)$$

Then

$$\langle J^* P_{\eta,F} Jf, g\rangle_\nu = \langle P_{\eta,F} Jf, Jg\rangle_\nu = \int_B \overline{Jg}(b) \left(\int_{u\in\pi^{-1}(b)} (f\circ\pi)((F^{-1}\circ\tilde{J})(u))d\eta_b(u) \right) d\nu(b)$$

$$= \int_B \int_{u\in\pi^{-1}(b)} (f\circ\pi)((F^{-1}\circ\tilde{J})(u))\overline{Jg}(\pi(u))d\eta_b(u)d\nu(b)$$

$$= \int_U (f\circ\pi)((F^{-1}\circ\tilde{J})(u))\overline{g}((J\circ\pi)(u))d\mu(u)$$

$$= \int_U (f\circ\pi)((F^{-1}\circ\tilde{J})(u))\overline{g}((\pi\circ\tilde{J})(u))d\mu(u)$$

Let $v = \tilde{J}(u)$ and use $\tilde{J}$-invariance of μ

$$= \int_U (f\circ\pi)((F^{-1}(v))\overline{g}(\pi(v)d\mu(v)$$

Let $w = F^{-1}(v)$ and use F-invariance of μ

$$= \int_U f(\pi(w))\overline{g}((\pi\circ F)(w))d\mu(w)$$

$$= \langle f, P_{\eta,F} g\rangle_\nu$$

as shown in the proof of 2.0.3

□

Now, suppose we have a third map $\tilde{S} : U \to U$ that shares the properties of $\tilde{J}$,

except that

2. $F\circ\tilde{S} = \tilde{S}\circ F$

Also assume the projections $J = S$.

Proposition 2.0.6. *Under the above assumption, $P_{\eta,F}$ commutes with J. Hence $P_{\eta,F}$*

is self-adjoint.

Proof.

$$\langle P_{\eta,F} Jf, g \rangle_\nu = \int_B \overline{g}(b) \left(\int_{u \in \pi^{-1}(b)} Jf((\pi \circ F)(u)) d\eta_b(u) \right) d\nu(b)$$

$$= \int_U f((J \circ \pi \circ F)(u)) \overline{g}(\pi(u)) d\mu(u)$$

$$= \int_U f((S \circ \pi \circ F)(u)) \overline{g}(\pi(u)) d\mu(u)$$

$$= \int_U f((\pi \circ \tilde{S} \circ F)(u)) \overline{g}(\pi(u)) d\mu(u)$$

$$= \int_U f((\pi \circ F \circ \tilde{S})(u)) \overline{g}(\pi(u)) d\mu(u)$$

Let $v = \tilde{S}(u)$ and use $\tilde{S}$-invariance of μ

$$= \int_U f((\pi \circ F)(v)) \overline{g}((\pi \circ \tilde{S}^{-1})(v)) d\mu(v)$$

$$= \int_U f((\pi \circ F)(v)) \overline{g}((S^{-1} \circ \pi)(v)) d\mu(v)$$

$$= \int_U f((\pi \circ F)(v)) \overline{g}((J^{-1} \circ \pi)(v)) d\mu(v)$$

$$= \int_B \overline{g}(J^{-1}(b)) \left(\int_{v \in \pi^{-1}(b)} f((\pi \circ F)(v)) d\eta_b(v) \right) d\nu(b)$$

$$= \int_B \overline{J^{-1}g}(b) \left(\int_{v \in \pi^{-1}(b)} f((\pi \circ F)(v)) d\eta_b(v) \right) d\nu(b)$$

$$= \langle P_{\eta,F} f, J^{-1} g \rangle_\nu$$

$$= \langle P_{\eta,F} f, J^* g \rangle_\nu$$

$$= \langle J P_{\eta,F} f, g \rangle_\nu$$

□

These are the results that we will need for the remainder of the thesis. Much more can be said about measured fibrations as a general construction.

2.3 Random Dynamical Systems Perspective

Typical developments of fiber bundles insist that all $\pi^{-1}(b)$ be homeomorphic, say to a space Q. This author believes that this is not strictly necessary to the theory that has been developed so far in this chapter, though we can typically accomplish it by simply finding a Q to embed each fiber into while leaving the support of η_b unchanged. Thus, the part that is added to the fiber is ignored, being a set of measure zero. We assume this going forward.

We may write a point $u \in U$ as $u = (b, q)$ and introduce the map

$$\Phi_q : B \to B$$

$$\Phi_q(b) = (\pi \circ F)(b, q)$$

Thus, the operator P_η can be written

$$(P_\eta f)(b) = \int_Q f(\Phi_q(b)) d\eta_b(q) \tag{2.10}$$

In the case $B = \mathbb{R}$ and if the "jumps" $\Phi_q(x) - x$ are not too big, we might restrict our attention to functions that allow us to expand as a power series and write

$$(P_\eta f)(x) = \int_Q f((\Phi_q(x) - x) + x) d\eta_x(q)$$

$$= \int_Q \left(f(x) + \frac{f'(x)}{1!}(\Phi_q(x) - x) + \frac{f''(x)}{2!}(\Phi_q(x) - x)^2 + \frac{f'''(x)}{3!}(\Phi_q(x) - x)^3 + ... \right) d\eta_x(q)$$

Thus, we are lead to consider the moments of Φ

$$M_j(b) = \int_Q (\Phi_q(b) - b)^j \, d\eta_b(q) \tag{2.11}$$

46

So that we can write

$$P_\eta f(x) - f(x) = \left(\int_Q f(\Phi_q(x)) d\eta_x(q) \right) - f(x)$$

$$= \int_Q \left(f(\Phi_q(x) - f(x) \right) d\eta_x(q)$$

$$= f'(x) M_1(x) + \frac{f''(x)}{2} M_2(x) + \frac{f'''(x)}{6} M_3(x) + \dots$$

Approximating the Markov operator by a differential operator may provide a tool to help understand the spectral properties of the operator and hence estimate rates of convergence. See chapter 4.

3. Gas-Surface Interaction With Moving Parts

In this chapter, we will describe the gas-surface interaction model with moving parts in detail. This model has been mentioned previously, but here we will be more concrete. It is inspired by and borrows from the kinetic theory of gases, but should be viewed as a mathematical system. It expands on the work of [1, 7, 8], which we will briefly describe.

For descriptive purposes, this chapter is meant to be largely self-contained. As such, some notions introduced previously in a broader context are presented again in a form more specifically targeted to the analysis of this particular model. We trust that reader will see how this description fits tightly with the larger theory.

Picture a gas particle confined to move in two dimensions in a long tube, as in figure 3.1. The particle reflects from the interior surface of the tube like a billiard ball. However, the surface of this tube is slightly rough. This <u>microstructure</u> causes the particle to scatter upon impact with the tube.

While the exact geometry of the microstructure can be varied to produce different models, we insist that it be <u>periodic</u> - composed of identical cells lining the tube's surface. The dimensions of these cells are tiny compared to the dimensions of the tube, and so are "invisible" to observers at the tube's size scale.
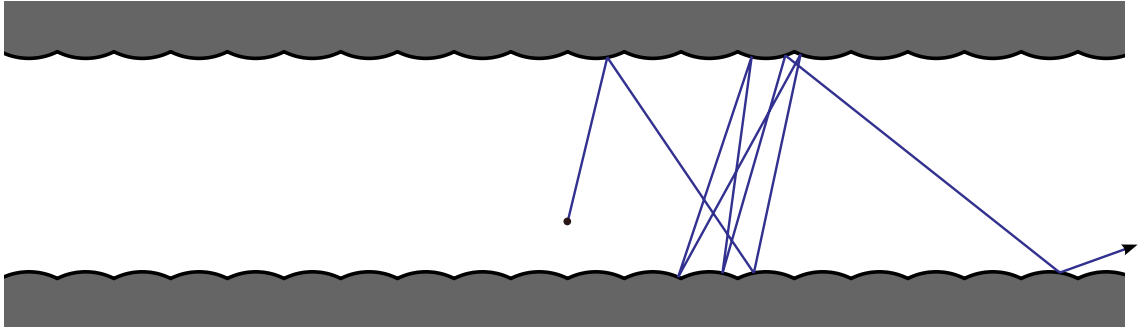
Figure 3.1. Tube with microstructure

Observe that a small difference in the point of impact makes a substantial difference in the angle of reflection. Given the scale of the microstructure, it would be experimentally impractical or impossible to measure the point of impact with enough precision to deterministically predict the outcome of the impact event. As previously discussed, we propose to treat as random those quantities that affect the outcome of an event but for which we have limited knowledge (either they can not be measured in principle or can not be measured with sufficient precision). Here, we assume the impact point is chosen uniformly at randomly

It is shown in [1] that this model induces a Markov chain which has a stationary distribution that follows Knudsen's Cosine Law and has nice spectral properties. We wish to expand on this work.

Now, we allow the "bumps" from the prior model to move perpendicularly to the surface of the tube. For clarity, we add vanishingly thin walls uniformly spaced perpendicular to the surface of the tube which partitions the surface into <u>cells</u>. Each

50

cell contains a bound particle confined to the cell; see figure 3.2. If desired, one can think of the bound particles as mathematically modeling the atoms comprising the surface of the tube, we consider several different shapes for the bound particle. An impact of the free particle with the surface of the tube is thus modeled as a sequence of collisions of the free particle with the side walls and bound particle of a cell. We call the dashed line the open wall of the cell. The free particle is said to enter or exit the cell when it crosses the open wall. The time between an entry and the next exit is an impact event.
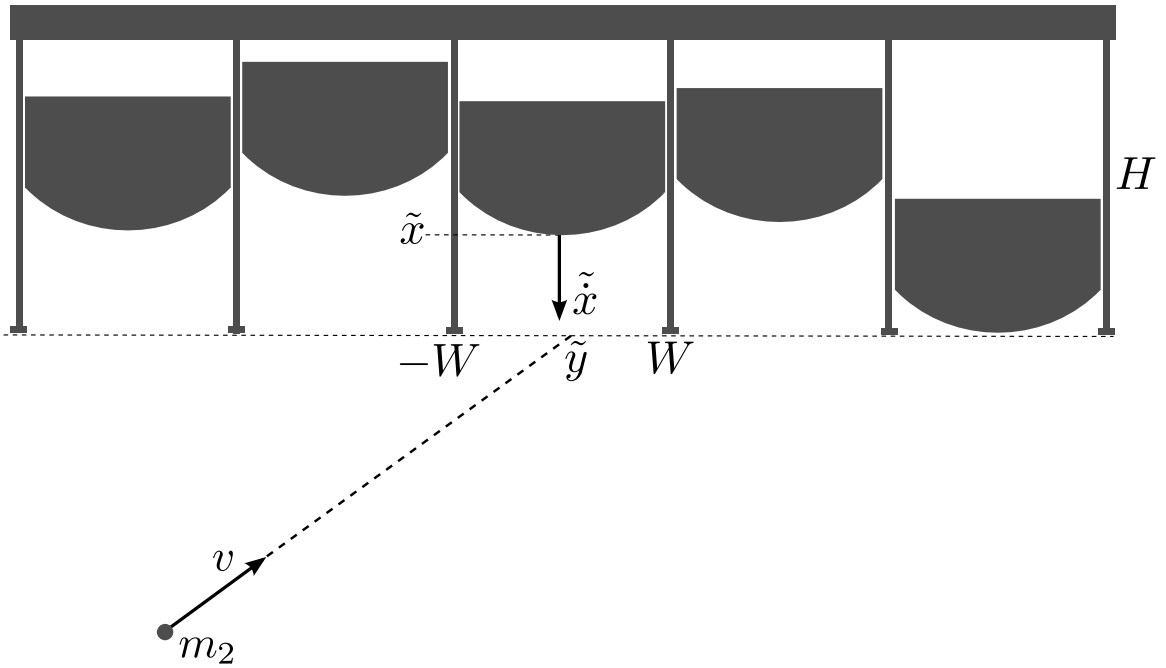
Figure 3.2. Top surface of the tube with circular moving parts

We have a recurring theme in this work of the interaction between the "macroscopic" and "microscopic". Our motivating interest lies in the macroscopic kinetic

Figure 3.3. Top surface of the tube with wedge shaped moving parts

information of the free particle, speed and angle of reflection, which an observer at the tube's size scale can see. However, our model asserts that these macroscopic quantities are produced by microscopic events which depend on information not readily accessible to the macroscopic observer. As a result, from the macroscopic viewpoint, the outcome of an impact event has a random distribution, while microscopically, the impact event is purely deterministic.

It may assist the reader to draw this dichotomy slightly farther. Once the free particle impacts the surface of the tube, a microscopic observer sees it enter a cell through the open wall, perform a sequence of collisions within the cell, and eventually leave the cell at a later time, at a different point of the open wall, and along a different

Figure 3.4. Top surface of the tube with flat moving parts

trajectory than at entry. However, a macroscopic observer sees the free particle reflect *immediately* and depart *from the same point*, since she can not resolve time and spatial differences at the scale of the cell. However, the two observers agree perfectly on the final trajectory of the free particle. We will place this description more squarely within the notions of chapter 1 below.

We will now describe the impact event from the microscopic viewpoint. During an impact event, the free particle is free to move in both dimensions and it collides specularly with the side walls. However, the bound particle will be constrained to move perpendicularly to the tube and will reverse direction but maintain speed (collide specularly) when it reaches either extreme of its cell. Particle-particle collisions obey

appropriate mechanical laws and allow the transfer of energy and momentum. This allows the free particle to reach thermal equilibrium with the tube over a sequence of impact event.

Since the free particle flies through the tube along straight line trajectories between impact events, we need only investigate the impact events. As before all cells are identical and the bound particles move independently. Hence, the only information preserved between impact events is the trajectory of the free particle. We ignore the possibility that the free particle returns to the same cell. Thus, it is convenient to think of our model as consisting of a sequence of impact events within the same cell, where the cell "resets" or "re-randomizes" each time the free particle reaches the open wall. For convenience, embed the cell into the yz-plane with the open wall along the horizontal y-axis and midpoint at the origin, opening downward.

This model has a number of parameters. First, the cell has a well defined height H and width $2W$. While the free particle is still treated as a point mass, the bound particle has a shape which is a parameter of the new model. We also need the mass ratio $\epsilon = \sqrt{\text{mass}_{\text{bound}}/\text{mass}_{\text{free}}}$. The tube has an average temperature T which will affect the speed of the bound particle.

In addition to the physical parameters, we have some random parameters. We treat the speed and angle of the free particle as observable variables. However, as before, the inital point of entry of the free particle into the cell is a hidden (random) variable. We also treat the initial position and velocity of the bound particle as hidden since the bound particle is a purely microscopic object and hence thoroughly invisible

to the (macroscopic) observer. The specific probability distributions for the random quantities are also parameters of the model. Note that all random choices are made simultaneous to the entry of the free particle into the cell.

The introduction of the bound particle complicates the nice billiard motion interpretation used in previous work. However, we can recover billiard motion by moving into $\mathbb{R}^3$ where a single <u>billiard ball</u> encodes the state of the cell as follows. The billiard ball is at position $\tilde{p} = (\tilde{x}, \tilde{y}, \tilde{z})$ and moving along trajectory $\tilde{v} = (\dot{\tilde{x}}, \dot{\tilde{y}}, \dot{\tilde{z}})$ where

$\tilde{x}$ = vertical position of bound particle

$\tilde{y}$ = horizontal position of free particle

$\tilde{z}$ = vertical position of free particle

$\dot{\tilde{x}}$ = vertical velocity of bound particle

$\dot{\tilde{y}}$ = horizontal velocity of free particle

$\dot{\tilde{z}}$ = vertical velocity of free particle

We call $(\tilde{p}, \tilde{v})$ the <u>state</u> of the billiard ball.

We can translate the physical constraints within the cell into inequalities on the coordinates of $\tilde{p}$. The exact inequalities depend upon the shape assigned to the bound particle and the point on the bound particle we use to specify its position.

For example, if the bound particle is flat as shown in figure 3.4 and, for maximal specificity, we track the bound particle's position at its midpoint, we have:

$$0 \leq \tilde{x} \leq H$$
$$-W \leq \tilde{y} \leq W \tag{3.1}$$
$$0 \leq \tilde{z} \leq \tilde{x}$$

If the bound particle is shaped like a downward opening wedge with exterior angle α as shown in figure 3.3, and we use the wedge point to specify its position, we have:

$$W \tan(\alpha) \leq \tilde{x} \leq H$$
$$-W \leq \tilde{y} \leq W \tag{3.2}$$
$$0 \leq \tilde{z} \leq \tilde{x} - |\tilde{y}| \tan(\alpha)$$

If the bound particle is shaped like a upward opening circle with curvature κ as shown in figure 3.2, and we use the circle's center to specify its position, we have:

$$1/\kappa \leq \tilde{x} \leq H + \sqrt{1/\kappa^2 - W^2}$$
$$-W \leq \tilde{y} \leq W \tag{3.3}$$
$$0 \leq \tilde{z} \leq \tilde{x} - \sqrt{1/\kappa^2 - \tilde{y}^2}$$

Clearly, there are many other possible interesting shapes for the bound particle. It is a continuing thrust of this research program to catalog the impact these selections have on the model's behavior.

These inequalities determine a chamber in $\mathbb{R}^3$ with piecewise smooth boundary components we will call <u>faces</u> (see figure 3.5). Then an impact event begins with the

billiard ball at a point $\tilde{p}$ on the face $\tilde{z} = 0$, moving along an intitial vector $\tilde{v}$ until it reaches another face. We want this collision to be specular so that we can use existing results about billiard motion. Sadly, as it stands, collisions with the face $\tilde{x} = \tilde{z}$ are not specular.
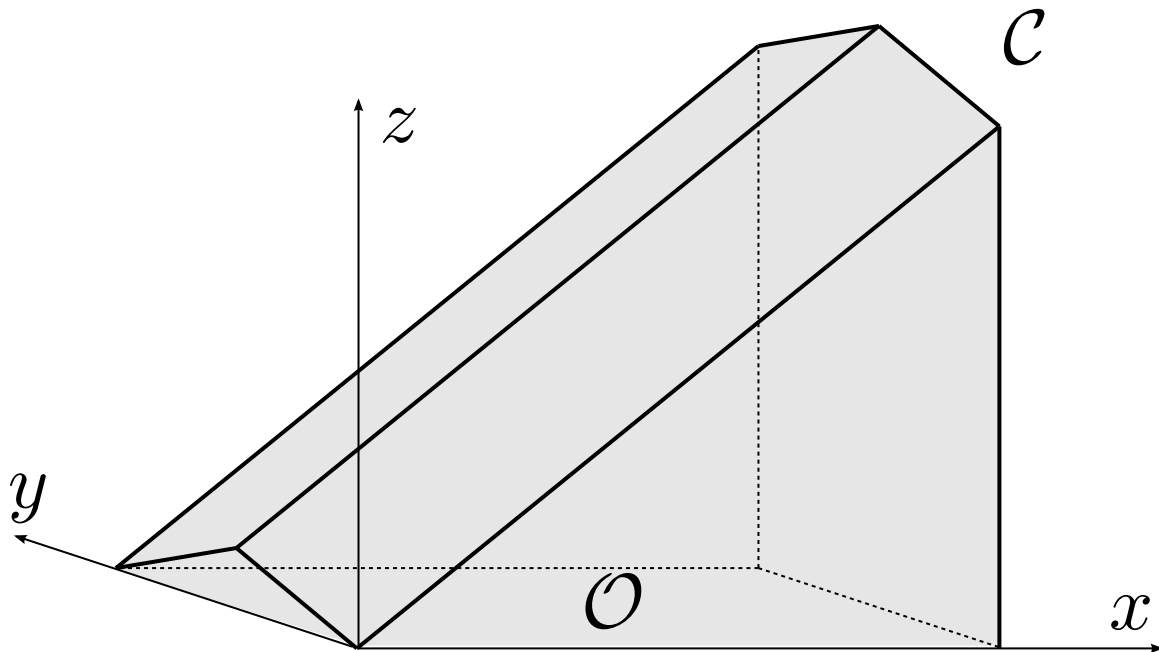
Figure 3.5. The billiard chamber associated to the gas-surface inter-action model with wedge-shaped moving parts.

But we can recover specular collisions and hence all of the prior Lagrangian me-chanical theory. Recall that in a specular collision, the component of the trajectory along the normal vector to the boundary at the collision point is reversed and the tangential components are preserved. In particular, the speed of the particle is un-changed. These notions are all defined in term of the standard Euclidean metric.

Observe that we have specular collisions at each face except $\tilde{x} = \tilde{z}$. For example, the billiard ball collides with face $\tilde{y} = W$ when the free particle collides with the rightmost wall of the cell. We said the free particle collides specularly with side walls, so this collision accomplishes $\dot{\tilde{y}} \mapsto -\dot{\tilde{y}}$. This is exactly specular collision for the billiard ball at this face. The same holds for all faces except $\tilde{x} = \tilde{z}$.

The billiard ball collides with face $\tilde{x} = \tilde{z}$ when the free particle and bound particle collide. We have conservation of kinetic energy.

$$\frac{1}{2}m_b\dot{\tilde{x}}_i^2 + \frac{1}{2}m_f(\dot{\tilde{y}}_i^2 + \dot{\tilde{z}}_i^2) = \frac{1}{2}m_b\dot{\tilde{x}}_o^2 + \frac{1}{2}m_f(\dot{\tilde{y}}_o^2 + \dot{\tilde{z}}_o^2) \tag{3.4}$$

where m_f and m_b are the masses of the free particle and bound particle respectively and i and o mean incoming (before collision) and outgoing (after collision) respectively. Multiplying by $2/m_f$ and recalling ϵ above

$$\epsilon^2\dot{\tilde{x}}_i^2 + \dot{\tilde{y}}_i^2 + \dot{\tilde{z}}_i^2 = \epsilon^2\dot{\tilde{x}}_o^2 + \dot{\tilde{y}}_o^2 + \dot{\tilde{z}}_o^2 \tag{3.5}$$

The ϵ^2 above means that the speed of the billiard ball is not conserved in the collision. So, we apply the transformation

$$\mathscr{T} := \begin{bmatrix} \epsilon & 0 & 0 \\ 0 & 1 & 0 \\ 0 & 0 & 1 \end{bmatrix}$$

This is a linear transformation, so it transforms points and vectors in the same way (the differential map for $\mathscr{T}$ is $\mathscr{T}$ itself). Letting $p = (x, y, z) := \mathscr{T}(\tilde{p})$ and $v = (\dot{x}, \dot{y}, \dot{z}) := \mathscr{T}(\tilde{v})$. We have

$$v_i \cdot v_i = \dot{x}_i^2 + \dot{y}_i^2 + \dot{z}_i^2 = (\epsilon \dot{\tilde{x}}_i)^2 + \dot{\tilde{y}}_i^2 + \dot{\tilde{z}}_i^2 =$$

$$= (\epsilon \dot{\tilde{x}}_o)^2 + \dot{\tilde{y}}_o^2 + \dot{\tilde{z}}_o^2 = \dot{x}_o^2 + \dot{y}_o^2 + \dot{z}_o^2 = v_o \cdot v_o$$

Thus, speed is conserved during the collision in the transformed space.

We call this transformed chamber the <u>billiard chamber</u> denoted $\mathcal{C}$. We will make no further reference to the untransformed space, except to note that the inequalities in 3.1, 3.2, and 3.3 can be modified slightly to give expressions for the faces of $\mathcal{C}$.

Note that the transformation $\mathscr{T}$ does not stretch in the y or z directions. This is convenient since $\dot{y}$ and $\dot{z}$ are the observable quantities. Hence, the quantities labeled y, z, $\dot{y}$ and $\dot{z}$ in the physical cell correspond to quantities in the billiard chamber $\mathcal{C}$ without modification, but

$x = \epsilon \cdot$vertical position of bound particle

$\dot{x} = \epsilon \cdot$vertical velocity of bound particle

The transformation by $\mathscr{T}$ only affects the nature of collision at face $x = z$; all other face still enjoy specular collisions. We claim that collisions at $x = z$ are specular and sketch a proof. Let τ be the tangent vector to the bound particle at the point where the free particle makes the collision. Then the momentum of the free particle parallel to τ and the total momentum of free particle and bound particle in the z-direction are conserved. In $\mathcal{C}$, these naturally correspond to independent vectors t_1

59

and t_2 in the tangent plane to $x = z$ at the collision point. Hence, these vectors are conserved in the collision. Combined with the condition that the billiard ball must stay inside $\mathcal{C}$, conservation of length (speed) and of these tangent vectors imply specularity of the collision. Hence all collisions in $\mathcal{C}$ are specular.

Let $\mathcal{O}$ be the open face $z = 0$ where an impact event begins and ends. Then an impact event is modeled on $\mathcal{C}$ by

1) Initialize - Select x, y, and $\dot{x}$ randomly. We know $z = 0$. And $\dot{y}$ and $\dot{z}$ come from the incoming state of the free particle

2) Perform billiard motion in $\mathcal{C}$ until the billiard ball returns to $\mathcal{O}$

3) Perform a final specular collision. Retain the values of $\dot{y}$ and $\dot{z}$ for the next impact event.

The final collision in step 3 is performed so that the billiard ball is traveling back into the billiard chamber for the next impact event. Recalling the full tube for a moment, if the free particle makes an impact on the top surface of the tube, it enters a downward opening cell with upward initial trajectory and downward departing trajectory. The next impact event will occur on the bottom surface with an upward opening cell. Thus, the second impact event is the axial reflection of the first impact event. The final collision in step 3 acounts for this reflection, allowing all impact events to be modeled on the same space $\mathcal{C}$.

In the general language of chapter 1, the billiard chamber $\mathcal{C}$ is the Riemannian manifold X and the open face $\mathcal{O}$ is the microscopic/macroscopic interface we called S. The potential function is constant (say zero for convenience). This is the special

case of billiard motion on the chamber $\mathcal{C}$ about which much is known, for example see [6] where one can see a careful argument of the fact that collisions made at edges and vertices of $\mathcal{C}$ can be safely ignored. We have intentionally oriented $\mathcal{C}$ in $\mathbb{R}^3$ so that we can use the particularly simple frame on $\mathcal{O}$ adapted to our choice of hidden and observable variables

$$e_1(p) \equiv \mathbf{i}$$

$$e_1'(p) \equiv \mathbf{j}$$

$$\mathbf{n}(p) \equiv \mathbf{k}$$

So, if the billiard ball completes an impact event with $v = (\dot{x}, \dot{y}, \dot{z})$, then the macroscopic observer sees the free particle reflect from the tube with speed $s = \sqrt{\dot{y}^2 + \dot{z}^2}$ and at angle $\tan(\varphi) = \dot{y}/\dot{z}$.

Some notes on terminology. Given that there are two spaces (the physical cell and the billiard chamber $\mathcal{C}$) with particles making collisions, I will attempt to use terms that keep these spaces distinct. Macroscopically, the free particle will *impact* the *surface* of the tube. Microscopically, our model views this as an *impact event* with the *cell*. The *particles collide* with the *walls* of the cell and each other. This is interpreted as billiard motion inside the *billiard chamber* where a single *billiard ball collides* with the *faces* of $\mathcal{C}$. Note that the term collide is reused (for lack of a third good synonym), but the other terms will (hopefully) be kept distinct and consistent to aid the reader.

Also, I will attempt to reserve the symbol φ for the "macroscopic" angle of reflection. For this model, φ is the angle of the free particle as it leaves the cell, with respect to the surface of the tube. It is an angle in the two dimensional yz-plane (relative to the z-axis). Then φ will be closely related to, but distinct from, the final trajectory of the billiard ball moving in $\mathcal{C}$. We will soon make us of the symbol ϕ in the sense of a polar angle in spherical coordinates as we analyze the billiard motion in $\mathcal{C}$. The symbols φ and ϕ have distinct meanings, but will be related.

4. Theoretical Investigation of the Moving Parts Model

In this chapter, we analyze the gas-surface interaction model with moving parts

4.1 Stationary Distribution for the Gaussian Model

In this section, we will finish the proof of theorem 1.1 begun in chapter 1. First, let us see how how it applies to the gas-surface interaction model with moving parts.

We identify the Riemannian manifold X as the billiard chamber $\mathcal{C}$, recalling that the metric is the Euclidean metric. The microscopic/macroscopic interface called S in the general theory is $\mathcal{O}$ in our model. The potential function $V(p) \equiv 0$ throughout $\mathcal{C}$, so that $r = \sqrt{2E(p,v)} = ||v||$. We have intentionally oriented $\mathcal{C}$ in $\mathbb{R}^3$ so that we can use the particularly simple frame on $\mathcal{O}$ adapted to our choice of hidden and observable variables

$$e_1(p) \equiv \mathbf{i}$$

$$e_1'(p) \equiv \mathbf{j}$$

$$\mathbf{n}(p) \equiv \mathbf{k}$$

Note that it is indeed true that the first $m_x = 1$ vectors of the frame correspond to the hidden variables, the next $m_y = 1$ vectors correspond to the observable variables, and $\mathbf{k}$ is normal to $\mathcal{O}$. Then the map G is simply the identity map.

To help the reader, we recall that on $\mathcal{O}$

$x = \epsilon*$ initial vertical position of bound particle

$y =$ initial horizontal position of free particle

$z = 0$

$\dot{x} = \epsilon*$ initial vertical velocity of bound particle

$\dot{y} =$ initial horizontal velocity of free particle

$\dot{z} =$ initial vertical velocity of free particle

Therefore, if we assert that x is chosen uniformly on its domain and that $\dot{x}$ is chosen according to a Gaussian distribution with mean 0 and variance σ^2, then corollary 1.1.1 applies. Thus, the stationary distribution ν is $N(0, \sigma)$ on $\dot{y}$, and $\chi_2(\sigma)$ on $\dot{z}$. If we switch to polar coordinates in the yz-plane, we get that the stationary distribution on the speed of the free particle is $\chi_3(\sigma)$ (Maxwell-Boltzmann in three dimensions) and on angle of reflection is $\cos\varphi d\varphi$ (the so-called Knudsen's Cosine Law).

We can easily generalize. Suppose the free particle moves in a three dimensional tube, making impacts with rectangular cells on the surface of the tube each containing a bound particle with a surface of some shape moving orthogonally to the tube. We simply add a second y variable, noting that the remainder of the argument works exactly the same. Provided that the initial position of the bound particle is uniform in the cell and its initial velocity is $N(0, \sigma)$, then the stationary distribution will be $\chi_4(\sigma)$ on speed of the free particle and $\cos\varphi d\omega_k^2$ on angle of reflection of the free

particle. Recall that ω_k^2 is the Riemannian volume form on $\mathbb{H}_1^2$, the upper half of the copy of S^2 sitting in the $\dot{x} = 0$ hyperspace of U.

We can easily go up many dimensions and in complexity of the cell (this is planned future work). Let us also point out this that works in lower dimension, such as in figure 1.1. Simply let $m_x = 0, m_x = 1$ and note that $\chi_3(\sigma)$ is trivially stationary for free particle speed (since speed does not change, any distribution is stationary) and $\cos \varphi d\varphi$ is stationary for angle.

The identification of the stationary distribution was a primary hurdle to the advancement of the understanding of this Markov chain. We already presented much of the reasoning that led to its discovery in chapter 1. What remains to prove theorem 1.1.

Theorem 4.1. *Let* $g(x) = \frac{1}{\sqrt{2\pi\sigma^2}} e^{-x^2/2\sigma^2}$ *and* $m(x) = \frac{1}{\sigma^2} x e^{-x^2/2\sigma^2}$. *Suppose the probability kernel* η *is given by*

$$\eta_{(\dot{\mathbf{y}}, \dot{z})} = (c_\eta \chi_r(p) d\omega_s) \left(\Pi_{i=1}^{m_x} g(\dot{x}_i) d\dot{x}_i \right)$$

Then the measure

$$\nu = \left(\Pi_{j=1}^{m_y} g(\dot{y}_j) d\dot{y}_j \right) (m(\dot{z}) d\dot{z})$$

on B *is* P_η-*stationary, where* c *normalizes. Changing to spherical coordinates on* B *and denoting the radius and polar angle by* s *and* φ *respectively, we obtain*

$$\nu = \left(c_\varphi \cos \varphi d\omega_k^{m_y} \right) \left(c_s s^{m_y+1} e^{-s^2/2\sigma^2} ds \right)$$

where the constants normalize.

Before beginning the proof, recall the following notations conventions: For notational brevity, write

$$\dot{\mathbf{x}} = (\dot{x}_1...\dot{x}_{m_x}) \in \mathbb{R}^{m_x}$$

$$\dot{\mathbf{x}}^2 = \dot{\mathbf{x}} \cdot \dot{\mathbf{x}}$$

$$d\dot{\mathbf{x}} = d\dot{x}_1...d\dot{x}_{m_x}$$

$$\dot{\mathbf{y}} = (\dot{y}_1...\dot{y}_{m_y}) \in \mathbb{R}^{m_y}$$

$$\dot{\mathbf{y}}^2 = \dot{\mathbf{y}} \cdot \dot{\mathbf{y}}$$

$$d\dot{\mathbf{y}} = d\dot{y}_1...d\dot{y}_{m_y}$$

Proof. From the definition of $\nu \circ \eta$, we see that

$$\nu \circ \eta = (c_\eta \chi_r(p) d\omega_s) \left(\Pi_{i=1}^{m_x} g(\dot{x}_i) d\dot{x}_i\right) \left(\Pi_{j=1}^{m_y} g(\dot{y}_j) d\dot{y}_j\right) (m(\dot{z}) d\dot{z})$$

$$= c_\eta \chi_r(p) \left(\Pi_{i=1}^{m_x} \frac{1}{\sqrt{2\pi\sigma^2}} e^{-\dot{x}_i^2/2\sigma^2}\right) \left(\Pi_{j=1}^{m_y} \frac{1}{\sqrt{2\pi\sigma^2}} e^{-\dot{y}_j^2/2\sigma^2}\right) \left(\frac{1}{\sigma^2} \dot{z} e^{-\dot{z}^2/2\sigma^2}\right) d\omega_s d\dot{\mathbf{x}} d\dot{\mathbf{y}} d\dot{z}$$

$$= c_\eta \chi_r(p) \left(\frac{1}{\sigma^2(2\pi\sigma^2)^{(m_x+m_y)/2}} e^{-r^2/2\sigma^2} r \cos\phi\right) d\omega_s \left(r^{n-1} d\omega_k^{n-1} dr\right)$$

$$= c_\eta \chi_r(p) \left(\frac{1}{\sigma^2(2\pi\sigma^2)^{(m_x+m_y)/2}} e^{-r^2/2\sigma^2} r \cos\phi\right) d\omega_s \left(r^{n-1} d\omega_k^{n-1} dr\right)$$

$$= (c_\eta \chi_r(p) d\omega_s) \left(c_\phi \cos\phi d\omega_k^{n-1}\right) \left(c_r r^n e^{-r^2/2\sigma^2} dr\right)$$

$$= \mu$$

where we have grouped the last line so that it is clear that, letting

$$\rho(r) = r^n e^{-r^2/2\sigma^2}$$

we see that μ is induced by the $(2n-1)$ form

$$\tau := \chi_r \omega_s \wedge \cos \phi \omega_k^{n-1} \wedge \rho(r)dr$$

This form is $G \circ R \circ G^{-1}$-invariant. Recall that we expressed the map G in spherical coordinates as

$$G(p,v) = (p, h(v), r(p,v)) = (G_r(p,v), r(p,v))$$

Since r is invariant under R, r is invariant under $G \circ R \circ G^{-1}$. Then recalling lemma 1.0.1, we have

$$(G \circ R \circ G^{-1})_*(\tau) = (G \circ R \circ G^{-1})_*(\chi_r \omega_s \wedge \cos \phi \omega_k^{n-1} \wedge \rho(r)dr))$$

$$= G_*(R_*(G_*^{-1}(\chi_r \omega_s \wedge \cos \phi \omega_k^{n-1}))) \wedge (G \circ R \circ G^{-1})_*(\rho(r)dr)))$$

$$= G_*(R_*\Omega_r) \wedge \rho(r)dr$$

$$= G_*(\Omega_r \wedge \rho(r)dr$$

$$= G_*(G_*^{-1}(\chi_r \omega_s \wedge \cos \phi \omega_k^{n-1}) \wedge \rho(r)dr$$

$$= \chi_r \omega_s \wedge \cos \phi \omega_k^{n-1} \wedge \rho(r)dr$$

$$= \tau$$

Thus τ is $G \circ R \circ G^{-1}$-invariant, as is the measure μ it induces. Then, by lemma 2.0.1, ν is P_η-stationary.

To see the last part of the theorem, we simply write ν in spherical coordinates in

B

$$\nu = \left(\Pi_{j=1}^{m_y} g(\dot{y}_j)d\dot{y}_j\right)\left(m(\dot{z})d\dot{z}\right)$$

$$= \left(\Pi_{j=1}^{m_y}\frac{1}{\sqrt{2\pi\sigma^2}}e^{-\dot{y}_j^2/2\sigma^2}\right)\left(\frac{1}{\sigma^2}\dot{z}e^{-\dot{z}^2/2\sigma^2}\right)d\dot{\mathbf{y}}d\dot{z}$$

$$= \left(\frac{1}{\sigma^2(2\pi\sigma^2)^{m_y/2}}e^{-s^2/2\sigma^2}s\cos\varphi\right)\left(s^{m_y}d\omega_k^{m_y}ds\right)$$

$$= \left(c_\varphi\cos\varphi d\omega_k^{m_y}\right)\left(c_s s^{m_y+1}e^{-s^2/2\sigma^2}ds\right)$$

$\square$

Thus, theorem 1.1.1 is proved.

4.2 Why Gaussian?

For our particular model, we can give a physical interpretation for the distributions chosen for x, y and $\dot{x}$. First, the free particle and bound particle are unrelated before the free particle enters the cell. Hence, the choices associated to the free particle should be made independent of those for the bound particle. Let's assume x and $\dot{x}$ are also independent since $V \equiv 0$.

Now, the motion of the bound particle should reflect the state of the bulk material (the tube) in which it is contained. Assuming that tube is itself stationary, the

distribution of initial bound particle velocity should have mean 0. If the tube has temperature T, we use the relationship

$$\overline{KE} = 3/2kT \tag{4.1}$$

from statistical physics and compute

$$T = \frac{2}{3k}\left(\overline{\frac{1}{2}m_{\text{bound}}v_{\text{bound}}^2}\right)$$
$$= \frac{1}{3k}\left(\overline{\epsilon^2 m_{\text{free}}(\dot{x}/\epsilon)^2}\right)$$
$$= \frac{m_{\text{free}}}{3k}\overline{\dot{x}^2}$$
$$\sigma^2 = \frac{3kT}{m_{\text{free}}}$$

Thus, σ is determined by the physical parameters.

Given these constraints, it makes sense to use the "most random" or "least knowledge" distribution. We can quantify this using the notion of entropy. Recall that the *entropy* of a continuous, real valued random variable X with density $q(x)$ is

$$H(X) = \int_{-\infty}^{\infty} q(x)\log q(x)dx \tag{4.2}$$

Since $\dot{x}$ is supported on all of $\mathbb{R}$, the maximal entropy choice is the Gaussian with mean 0 and variance σ^2. Similarly, x and y must be compactly supported so that the maximal entropy distribution is uniform on the support.

Now, we certainly can impose other distributions on the hidden variables and investigate the effects on the induced stationary distribution. In fact, this is the path this investigation took chronologically. Later in this chapter and the next, we will

see explore Gaussian distributions on $\dot{x}$. We will see that we can recover Maxwell-Boltzmann in the limit $\epsilon \to \infty$, but that the stationary distribution can be far from Maxwell-Boltzmann for moderate values of ϵ.

4.3 Self-Adjoint

Now, we want to show that the Markov chain associated to the Gaussian model is self-adjoint. To ths end, we produce the maps $\tilde{J}$ and $\tilde{S}$ discussed in chapter 2, so that proposition 2.0.6 applies to show that the chain in indeed self-adjoint.

We will do the first half of this argument in the general

Consider the map $\tilde{J} : U \to U$ given by

$$\tilde{J}(x, y, \dot{x}, \dot{y}, \dot{z}) = (x, y, -\dot{x}, -\dot{y}, \dot{z})$$

We call this the <u>flip map</u> because it reverses the trajectory of the particle in the sense below. Recall that the particle first returns to $\mathcal{O}$ along a trajectory with $\dot{z} < 0$, but that we perform one final collision when it reaches $\mathcal{O}$ in order to properly set up the next impact event. This final collision merely changes the sign of $\dot{z}$. One may consider $\tilde{J}$ to first undo this negation of $\dot{z}$ and then negate every component of the trajectory, thus flipping the final trajectory.

We'd like to confirm that this map has all the properties needed for proposition 2.0.5. Before we begin, quickly recall the calculus fact that if g is an even function, then $\int_{-a}^{a} f(-x)g(x)dx = \int_{-a}^{a} f(x)g(x)dx$ by letting $u = -x$.

1. $\tilde{J}$ is invertible

   It is its own inverse

2. $R \circ \tilde{J} = \tilde{J} \circ R^{-1}$

   Consider the following sequence of operations. From an intial entry state (p, v), follow the billiard motion until first return to $\mathcal{O}$. Flip the final trajectory. Follow the billiard motion until second return to $\mathcal{O}$. The particle must be at the original point. Flip the final trajectory. The new trajectory must be the original trajectory. Hence

$$\tilde{J} \circ R \circ \tilde{J} \circ R = I \text{ and } R \circ \tilde{J} = \tilde{J}^{-1} \circ R^{-1} = \tilde{J} \circ R^{-1}$$

   This is a general statement of time reversibility.

3. $\tilde{J}$ projects to a map $J : B \to B$; that is $(J \circ \pi) = (\pi \circ \tilde{J})$

   Since π is projection onto the observable coordinates, clearly

$$J(\dot{y}, \dot{z}) = (-\dot{y}, \dot{z})$$

4. $\mu = \nu \circ \eta$ is $\tilde{J}$-invariant (as well R-invariant)

Then for $f : U \to \mathbb{R}$, compute

$$\mu(f) = c \int_{\mathcal{O}} \int_{\dot{x} \in \mathbb{R}} \int_{\dot{y} \in \mathbb{R}} \int_{\dot{z} \in \mathbb{R}^+} f(x, y, \dot{x}, \dot{y}, \dot{z}) e^{-\dot{x}^2/2\sigma^2} e^{-\dot{y}^2/2\sigma^2} \dot{z} e^{-\dot{z}^2/2\sigma^2} d\dot{x} d\dot{y} d\dot{z} dx dy$$

$$= c \int_{\mathcal{O}} \int_{\dot{x} \in \mathbb{R}} \int_{\dot{y} \in \mathbb{R}} \int_{\dot{z} \in \mathbb{R}^+} f(x, y, -\dot{x}, -\dot{y}, \dot{z}) e^{-\dot{x}^2/2\sigma^2} e^{-\dot{y}^2/2\sigma^2} \dot{z} e^{-\dot{z}^2/2\sigma^2} d\dot{x} d\dot{y} d\dot{z} dx dy$$

$$= c \int_{\mathcal{O}} \int_{\dot{x} \in \mathbb{R}} \int_{\dot{y} \in \mathbb{R}} \int_{\dot{z} \in \mathbb{R}^+} f(\tilde{J}(x, y, \dot{x}, \dot{y}, \dot{z})) e^{-\dot{x}^2/2\sigma^2} e^{-\dot{y}^2/2\sigma^2} \dot{z} e^{-\dot{z}^2/2\sigma^2} d\dot{x} d\dot{y} d\dot{z} dx dy$$

$$= \mu(f \circ \tilde{J})$$

$$= (\tilde{J}_* \mu)(f)$$

where the second line uses the fact twice.

5. $\pi \circ \tilde{J}^{-1} = J^{-1} \circ \pi$

Both equal J

Hence, by proposition 2.0.5, we have $P^*_{\eta,R} = J^* P^*_{\eta,R} J$.

Now, the particular bound particle shapes we considered chapter 3 are symmetric about $y = 0$. Thus, for these specific systems, we consider the map

$$\tilde{S}(x, y, \dot{x}, \dot{y}, \dot{z}) = (x, -y, \dot{x}, -\dot{y}, \dot{z}) \tag{4.3}$$

We confirm the properties required of this map in proposition 2.0.6.

1. $\tilde{S}$ is invertible.

In fact, $\tilde{S}$ is an involution.

2. $R \circ \tilde{S} = \tilde{S} \circ R$

To see this, consider the two sequences of operations below. One may either

think about the billiard ball in $\mathcal{C}$ or the two particles in the physical cell. From an intial state (p, v), either:

(a) Perform an impact event

(b) Reflect across $y = 0$, perform an impact event, Reflect across $y = 0$

Both processes yield the same final state, under the bilateral symmetry assumption. Then

$$R = \tilde{S} \circ R \circ \tilde{S} \text{ and } R \circ \tilde{S} = \tilde{S}^{-1} \circ R = \tilde{S} \circ R \tag{4.4}$$

3. $\tilde{S}$ projects to a map $S : B \to B$

$$S(\dot{y}, \dot{z}) = (-\dot{y}, \dot{z}) \tag{4.5}$$

4. $\mu = \nu \circ \eta$ is $\tilde{S}$-invariant

$$
\begin{aligned}
\mu(f) &= c \int_{\mathcal{O}} \int_{\dot{x} \in \mathbb{R}} \int_{\dot{y} \in \mathbb{R}} \int_{\dot{z} \in \mathbb{R}^+} f(x, y, \dot{x}, \dot{y}, \dot{z}) e^{-\dot{x}^2/2\sigma^2} e^{-\dot{y}^2/2\sigma^2} \dot{z} e^{-\dot{z}^2/2\sigma^2} d\dot{x} d\dot{y} d\dot{z} dx dy \\
&= c \int_{\mathcal{O}} \int_{\dot{x} \in \mathbb{R}} \int_{\dot{y} \in \mathbb{R}} \int_{\dot{z} \in \mathbb{R}^+} f(x, -y, \dot{x}, -\dot{y}, \dot{z}) e^{-\dot{x}^2/2\sigma^2} e^{-\dot{y}^2/2\sigma^2} \dot{z} e^{-\dot{z}^2/2\sigma^2} d\dot{x} d\dot{y} d\dot{z} dx dy \\
&= c \int_{\mathcal{O}} \int_{\dot{x} \in \mathbb{R}} \int_{\dot{y} \in \mathbb{R}} \int_{\dot{z} \in \mathbb{R}^+} f(\tilde{S}(x, y, \dot{x}, \dot{y}, \dot{z})) e^{-\dot{x}^2/2\sigma^2} e^{-\dot{y}^2/2\sigma^2} \dot{z} e^{-\dot{z}^2/2\sigma^2} d\dot{x} d\dot{y} d\dot{z} dx dy \\
&= \mu(f \circ \tilde{S}) \\
&= (\tilde{S}_* \mu)(f)
\end{aligned}
$$

where the second line uses the fact twice (using the characteristic function of the domain of y for the y integral).

5. $\pi \circ \tilde{S}^{-1} = S^{-1} \circ \pi$

Both equal S

(*) $J = S$

Yes.

Hence, by proposition 2.0.6, we have $P_{\eta,R}$ is self-adjoint on $L^2(B, \nu)$.

4.4   Approximation by Differential Operators

Recall that we saw at the end of chapter 2 the idea to approximate our operator

by a differential operator

$$(P_\eta f)(x) = \int_Q f((\Phi_q(x) - x) + x) d\eta_x(q)$$

$$= \int_Q \left(f(x) + \frac{f'(x)}{1!}(\Phi_q(x) - x) + \frac{f''(x)}{2!}(\Phi_q(x) - x)^2 + \frac{f'''(x)}{3!}(\Phi_q(x) - x)^3 + ... \right) d\eta_x(q)$$

$$= f(x) + f'(x)M_1(x) + \frac{f''(x)}{2}M_2(x) + \frac{f'''(x)}{6}M_3(x) + ...$$

Let us put this idea into action on the moving parts model where the initial

velocity of the bound particle is not assumed to be Gaussian. Let the bound particle

be flat, as in figure 3.4. Then the billiard chamber $\mathcal{C}$ will be similar to the one

presented in figure 3.5 except the top will be flat, rather than wedge shaped. If, in

addition, the free particle is initially moving strictly vertically ($\dot{y} = 0$), then it can

never gain any horizontal velocity. Then $\dot{y} = 0$ always and this is billiard motion in a

two dimensional plane $y =$ constant. Then the billiard chamber is a triangular billiard

table and $\dot{z}$ is the only observable variable. For convenience, we take the height of

the cell $H = 1$. Thus $\mathcal{C}$ is the triangle in the xz-plane shown in 4.1.

Now, we assume that x is chosen uniformly, but do not assume any specific distribution on $\dot{x}$. We assume it is continuous with density $\beta(\dot{x})$. Let us assume that β is an even function of $\dot{x}$. In particular, the mean of $\dot{x}$ is zero and we will consider the trajectories in equal probability pairs $(\dot{x}, \dot{z})$ and $(-\dot{x}, \dot{z})$, so that we only deal with $\dot{x} \geq 0$. Denote the variance of β by σ^2.

As discussed before, if the free particle has initial velocity $\dot{z}$, an impact event involves an initial choice of x and $\dot{x}$, giving the initial state

$$(p^{in}, v^{in}) = (x^{in}, \dot{x}^{in}, \dot{z}^{in})$$

The billiard ball then executes billiard motion in the chamber until it returns to the open face $z = 0$ in the final state

$$(p^{out}, v^{out}) = (x^{out}, \dot{x}^{out}, \dot{z}^{out})$$

The final macroscopic trajectory of the free particle is obtained by reflection once more and taking the dot product of the kinetic part with the inward pointing unit normal vector at that point. Alternately, we dot with the outward unit normal with no final reflections.
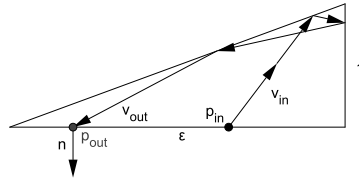
Figure 4.1. A shot in the triangle associated to strictly vertical motion of the two particles. Note the mass ratio ϵ determines the length of the base.

75

We wish to track the billiard motion through $\mathcal{C}$. Since the billiard ball can potentially make a large number of collisions during an impact event, it will simplify the process to introduce the idea to unfold the table. When the billiard ball makes a collision with a face of the table, rather than reflecting its path, we reflect the entire table about that face and allow the billiard ball to continue along its prior straight line path. We continue reflecting the table until the billiard ball finally reaches a reflection of the open side $\mathcal{O}$. At this point, we simply take the dot product of the trajectory with the outward pointing unit normal at that point. See figure 4.2

Now, rather than unfolding the table one reflection at a time as the particle travels as described above, we simply fully unfold the table before the impact event so that any possible path of the billiard ball is enclosed by the unfolded table. Note that the unfolded table has two sheets, one for each of the two "closed" faces. The billiard ball takes the one associated to the face it first collides against.

For small values of ϵ, we need a large number of unfolding to enclosed all trajectories. However, if $\epsilon \geq \sqrt{3}$, three reflections suffice to enclose all billiard ball trajectories.
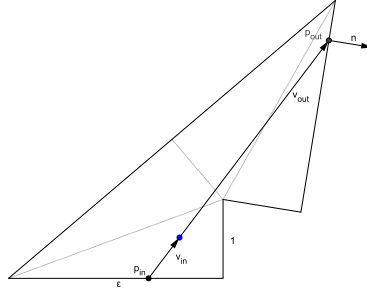
Figure 4.2. I am sorry - this image did not turn out well and I have not been able to fix it. You can easily do this yourself with Geogebra.

Now observe that if $\dot{x} > 0$ and the ratio $\frac{\dot{z}}{\dot{x}} \leq \frac{1}{\epsilon}$, then a billiard ball moving along trajectory $(\dot{x}, \dot{z})$ collides with face 1 with probability 1 and along the trajectory $(-\dot{x}, \dot{z})$ with face 3 with probability 1. We easily compute the normal vectors

$$n_1 = (\frac{2\epsilon}{1 + \epsilon^2}, -\frac{1 - \epsilon^2}{1 + \epsilon^2})$$

$$n_3 = (-\frac{2\epsilon}{1 + \epsilon^2}, -\frac{1 - \epsilon^2}{1 + \epsilon^2})$$

So that both trajectories result in the same outcome

$$T_1(\dot{x}, \dot{z}) = \frac{2\epsilon}{1 + \epsilon^2}\dot{x} - \frac{1 - \epsilon^2}{1 + \epsilon^2}\dot{z}$$

Now, if $\frac{\dot{z}}{\dot{x}} > \frac{1}{\epsilon}$, the trajectory $(-\dot{x}, \dot{z})$ still collides with face 3 with probability 1, but the trajectory $(\dot{x}, \dot{z})$ might hit any of the three faces depending on the launch point x (for steep angles, face 2 eventually becomes unreachable). If the launch point is within $\frac{\dot{x}}{\dot{z}}$ of the right side of the open face, then the $(\dot{x}, \dot{z})$ trajectory takes the clockwise sheet and collides with face 1. So the probability of this event is $\frac{1}{\epsilon}\frac{\dot{x}}{\dot{z}}$. If the

77

launch point is outside of this region, the $(\dot{x}, \dot{z})$ trajectory may hit face 2 or face 3.
Since the $\dot{x}$-component of this trajectory is positive, the latter option gives a second
possible outcome

$$T_2(\dot{x}, \dot{z}) = -\frac{2\epsilon}{1 + \epsilon^2}\dot{x} - \frac{1 - \epsilon^2}{1 + \epsilon^2}\dot{z}$$

Note the sign flip. Now the $(\dot{x}, \dot{z})$ trajectory might also hit face 3. But, as $\epsilon \to \infty$,
this is increasingly unlikely, so for simplicity, we ignore this possibility and proceed
as though it hit facel 3 instead. Furthermore, we now replace the maps T_1 and T_2 by
their asymptotic approximations

$$T_1(\dot{x}, \dot{z}) = \frac{2}{\epsilon}\dot{x} + (1 - \frac{2}{\epsilon^2})\dot{z} := b\dot{x} + (1 + a)\dot{z}$$
$$T_2(\dot{x}, \dot{z}) = -\frac{2}{\epsilon}\dot{x} + (1 - \frac{2}{\epsilon^2})\dot{z} := -b\dot{x} + (1 + a)\dot{z}$$

And their probabilities of being applied are

$$P_1(\dot{x}, \dot{z}) = \begin{cases} \frac{1}{2} + \frac{1}{2}\frac{1}{\epsilon}\frac{\dot{x}}{\dot{z}}, & \text{if } \dot{x} \leq \epsilon\dot{z} \\ 1, & \text{if } \dot{x} > \epsilon\dot{z} \end{cases} = \begin{cases} \frac{1+p}{2} & \text{if } \dot{x} \leq \epsilon\dot{z} \\ 1, & \text{if } \dot{x} > \epsilon\dot{z} \end{cases}$$

$$P_2(\dot{x}, \dot{z}) = \begin{cases} \frac{1-p}{2} & \text{if } \dot{x} \leq \epsilon\dot{z} \\ 0, & \text{if } \dot{x} > \epsilon\dot{z} \end{cases}$$

So, recalling the definition of the moments of P, we can write

$$M_j(\dot{z}) = \int_Q (\Phi_q(\dot{z}) - \dot{z})^j \, d\eta_{\dot{z}}(q)$$

$$= \int_{\dot{x} \in \mathbb{R}} \int_{x \in \mathcal{O}} ((\Phi_{x,\dot{x}}(\dot{z}) - \dot{z})^j \, d\eta_{\dot{z}}(x, \dot{x})$$

$$= \int_0^\infty \left(P_1(\dot{x}, \dot{z}) \, (T_1(\dot{x}, \dot{z}) - \dot{z})^j + P_2(\dot{x}, \dot{z}) \, (T_2(\dot{x}, \dot{z}) - \dot{z})^j \right) \beta(\dot{x}) d\dot{x}$$

$$= \int_0^{\epsilon\dot{z}} \left(\frac{1+p}{2} \, (b\dot{x} + a\dot{z})^j + \frac{1-p}{2} \, (-b\dot{x} + a\dot{z})^j \right) \beta(\dot{x}) d\dot{x} + \ldots$$

$$\ldots + \int_{\epsilon\dot{z}}^\infty (b\dot{x} + a\dot{z})^j \, \beta(\dot{x}) d\dot{x}$$

Then

$$M_1(\dot{z}) = \int_0^{\epsilon\dot{z}} a\dot{z}\beta(\dot{x})d\dot{x} + \int_0^{\epsilon\dot{z}} pb\dot{x}\beta(\dot{x})d\dot{x} + \int_{\epsilon\dot{z}}^\infty b\dot{x}\beta(\dot{x})d\dot{x} + \int_{\epsilon\dot{z}}^\infty a\dot{z}\beta(\dot{x})d\dot{x}$$

$$= a\dot{z} \int_0^{\epsilon\dot{z}} \beta(\dot{x})d\dot{x} + \frac{b}{\epsilon\dot{z}} \int_0^{\epsilon\dot{z}} \dot{x}^2\beta(\dot{x})d\dot{x} + b \int_{\epsilon\dot{z}}^\infty \dot{x}\beta(\dot{x})d\dot{x} + a\dot{z} \int_{\epsilon\dot{z}}^\infty \beta(\dot{x})d\dot{x}$$

Combine the first and last terms to get $a\dot{z}$ since β is a probability measure. As $\epsilon \to \infty$, the second term approaches the variance of β and the third vanishes. Hence

$$M_1(\dot{z}) = a\dot{z} + \frac{b\sigma^2}{\epsilon\dot{z}} = \frac{2}{\epsilon^2} \left(\frac{\sigma^2}{\dot{z}} - \dot{z} \right)$$

Similarly

$$M_2(\dot{z}) = \int_0^{\epsilon\dot{z}} b^2\dot{x}^2\beta(\dot{x})d\dot{x} + \int_0^{\epsilon\dot{z}} a^2\dot{z}^2\beta(\dot{x})d\dot{x} + \int_0^{\epsilon\dot{z}} 2pab\dot{x}\dot{z}\beta(\dot{x})d\dot{x} + ...$$

$$... + \int_{\epsilon\dot{z}}^{\infty} b^2\dot{x}^2\beta(\dot{x})d\dot{x} + \int_{\epsilon\dot{z}}^{\infty} a^2\dot{z}^2\beta(\dot{x})d\dot{x} + + \int_{\epsilon\dot{z}}^{\infty} 2ab\dot{x}\dot{z}\beta(\dot{x})d\dot{x}$$

$$= b^2\sigma^2 + a^2\dot{z}^2 + \frac{2ab\sigma^2}{\epsilon}$$

$$= \frac{2}{\epsilon^2}\left(2\sigma^2 + \frac{2}{\epsilon^2}\dot{z} - \frac{4}{\epsilon^2}\sigma^2\right) \to \frac{2}{\epsilon^2}\left(2\sigma^2\right)$$

Note that we have pulled the same power of ϵ from both moments. A quick calculation shows that the higher moments all decay like $\frac{1}{\epsilon^3}$. So let

$$L(f) := \sigma^2 f''(\dot{z}) + \left(\frac{\sigma^2}{\dot{z}} - \dot{z}\right)f'(\dot{z}) \tag{4.6}$$

Writing P_ϵ for the Markov operator associated for the model with mass ratio ϵ, we approximate

$$\frac{\epsilon^2}{2}(P_\epsilon f - f) \approx L(f) \tag{4.7}$$

Note that we can rewrite as

$$L(f) := \frac{1}{\rho}\frac{\partial}{\partial\dot{z}}\left(\rho\frac{\partial f}{\partial\dot{z}}\right) \tag{4.8}$$

where $\rho(\dot{z}) = \frac{1}{\sigma^2}\dot{z}e^{-\dot{z}^2/2\sigma^2}$. We recognize the form of the classical theory of Sturm-Liouville equations. Much is known about such operators; in particular, they have a nice spectral theory that might be used to approximate the spectrum of P_ϵ. It is a future project in this research to understand the precise conditions and methods for performing such a spectral approximation. See [1] for an example of this approach.

In particular, we'd like to show here how this approach produces the Maxwell-Boltzmann distribution. Assume the boundary conditions already discussed (goes to

0 at 0 and ∞ and has vanishing derivative at ∞). A quick computation shows that, with these conditions, on the space $L^2([0, \infty), \lambda)$ where λ is Lebesgue measure, the adjoint of a second order differential operator

$$L = a_2(x)\frac{\partial^2}{\partial x^2} + a_1(x)\frac{\partial}{\partial x}$$

$$L^* = a_2(x)\frac{\partial^2}{\partial x^2} - a_1'(x)\frac{\partial}{\partial x}$$

Observe

$$L_\epsilon^* f = 0 \implies \sigma^2 f'' = \left(\left(\frac{\sigma^2}{\dot{z}} - \dot{z}\right) f(\dot{z})\right)'$$

$$\implies \sigma^2 f' = \left(\left(\frac{\sigma^2}{\dot{z}} - \dot{z}\right) f(\dot{z})\right) + c_1$$

$$\implies \frac{f'}{f} = \frac{1}{\dot{z}} - \frac{\dot{z}}{\sigma^2}$$

$$\implies \ln(f) = \ln(\dot{z}) - \frac{\dot{z}^2}{2\sigma^2} + c$$

$$\implies f = c\dot{z}e^{-\frac{\dot{z}^2}{2\sigma^2}}$$

$$\implies f = \frac{1}{\sigma^2}\dot{z}e^{-\frac{\dot{z}^2}{2\sigma^2}}$$

where $c_1 = 0$ by the boundary assumptions. Hence, in the limit, $P_\epsilon^* f = f$. This helps to provide some explanation for the numerical observation in the next chapter that in the limit as $\epsilon \to \infty$, the Maxwell-Boltzmann is seen as the stationary distribution for free particle speed under more general assumptions on the distribution of the hidden kinetic variables than Gaussian.

4.5 Summary

In this chapter, we have proven lemma 1.1 which immediately proves that the Maxwell-Boltzmann distribution of appropriate dimension is stationary for speed and the area measure on the upper half sphere times cosine of the polar angle is stationary for angle *assuming that the hidden kinetic variables are distributed according to the Gaussian distribution with mean 0 and variance σ^2* and the spatial variables are distributed uniformly. This result holds under all choices of physical parameters. This provides a common Hilbert space on which to compare the operators associated to the various choices of the parameters. This will be a next step in this work.

We have also used the method of approximation by differential operators on the two dimensional version of the moving parts model. The fact that we can produce the Maxwell-Boltzmann distribution in the limit as $\epsilon \to \infty$ provides good evidence for the future utility of this method. We are optimistic that it will allow us to explore the more subtle properties of our Markov operators, in particular the spectral properties which control the rate of convergence of the Markov chain. We would like to know if the particular choices of bound particle shape and mass will impact the spectrum of the resulting operator.

In the next chapter, we will see the results of some numerical simulation studies which move us down that road.

5. Numerical Investigations

In this chapter, we discuss simulation studies of various versions of the gas-surface interaction model with moving parts. Since there are a large number of parameters within the model, we will choose to focus our attention on the effect of changing the shape of the bound particle, the value of the ratio of masses ϵ, and the distribution from which the initial velocity of the bound particle is drawn. In this chapter, we fix the values

$$\sigma = 2$$

$$\text{mass}_{\text{free}} = m_f = \frac{3}{4}$$

$$\text{cell half width} = W = 1$$

$$\text{cell height} = H = 5$$

The initial positions of the particles are always chosen uniformly on the domain.

5.1   Brief Description of Simulation Method

As part of this thesis work, I wrote a program in C++ to simulate sequences of impact events. The C++ program writes a file containing the sequence of post-impact

speed of angles of the free particle. This file is then read into Matlab and a finite rank approximation of the transition operator is computed as discussed below.

Forthcoming work of Renato Feres and Hong-Kun Zhang suggests that our operator should be a compact operator and hence well approximated by finite rank approximation. In particular, this means the spectral information provided numerically here should reflect the true operator. It is a future project to explore the operator theoretic details of the model in further detail.

A single simulation is divided into multiple <u>trials</u>, which consist of the following steps:

1. Establish the initial values of speed and angle of the free particle

2. Perform an impact event

3. Write the resulting speed and angle of the free particle to the file

4. Repeat 1-3 a fixed number of times (typically 100,000 impact events), with the final speed and angle of the free particle from the prior impact event used as the initial values for the next impact event

Often we let the first trial in a simulation be very long (5,000,000 impact events) to help accurately establish the range of possible values for the observed variables.

After a trial is completed in the C++ simulator, the data is analyzed in Matlab. The central process of the Matlab analysis is the computation of a finite rank approximation of the transition operator of the Markov chain. The sequences of angles and

speed are separately subjected to the following steps

After the first trial of a simulation only

1. Establish the range of values (the interval between the minimum and maximum value appearing in the data)

2. Subdivide this interval into N equal length pieces, or <u>bins</u> (typically, $N = 100$). This is the rank of the approximation.

   After all trials of a simulation

3. Bin data from the most recent trial (the new data)

4. Compute the transition count matrix of the new data - the $N \times N$ matrix A where $a_{i,j} =$ number of times that a value falling in the ith bin is immediately followed by a value falling in the jth bin

5. Add the new transition count matrix to the transition count matrix computed in prior trial (cumulative)

6. Normalize so that all rows sum to 1 (unless all entries are 0)

7. Compute (left) eigenvalues and eigenvectors of this rank N approximation to the Markov operator

The density function for the stationary distribution is well approximated by the step function $\sum_{i=1}^{N} v_i \mathbb{1}_i(x)$ where v_i is the ith entry of the eigenvector associated to the largest eigenvalue, 1, and $\mathbb{1}_i$ is the indicator function of bin i.

The function "eigs" in Matlab yields better results as the number of rows containing all zeros decreases. Hence, the initial values of speed and angle for the next trial are chosen as the midpoint of the bin corresponding to the row of the transition count matrix with the smallest row sum. This ensures that the row sum of this row will be at least 1 after the next trial.

5.1.1 How to read these plots

Each of the following plots involves a choice of

1. Initial distribution of $\dot{x}$

2. Shape of bound particle

3. Which variable (angle or speed of free particle) is plotted on the x-axis

This information is printed in the title. As one moves down a column, the value of $\epsilon = \sqrt{\text{mass}_{\text{bound}}/\text{mass}_{\text{free}}}$ increases with the geometric parameter (either the exterior angle α for a wedge shaped bound particle or the curvature of a circular shaped bound particle) fixed. As one move across a row, the value of the geometric parameter increases and ϵ remains fixed. In general, we are most interested in limiting behavior as the geometric parameter approaches zero (a flat bound particle) and as ϵ either approaches zero or infinity.

5.2   The Gaussian Model

We showed in chapter 4 that any model where $\dot{x}$ is chosen according to a Gaussian with mean 0 and standard deviation σ produces $MB_3(\sigma)$ and $\cos\varphi$ as stationary distributions for speed and angle of the free particle resp.. Thus, we include the following plots simply to validate the simulation. Consider figure 5.1 and figure 5.2. For a variety of bound particle geometries and values of ϵ, the simulation data perfectly reflects the expected behavior.

5.3   The Uniform Model

Now, suppose $\dot{x}$ is chosen according to the uniform distribution on $[-\sqrt{3}\sigma, \sqrt{3}\sigma]$. Note that this interval is chosen so that the standard deviation of this distribution is σ. First, we consider the stationary distributions of the angle of reflection for the two bound particle shapes then we show the stationary distributions for speed.

5.4   The Bernoulli Model

Now, suppose $\dot{x}$ is chosen according to the Bernoulli distribution on $\{-\sigma, \sigma\}$. Note again that this domain is chosen so that the standard deviation of this distribution is σ. First, we consider the stationary distributions of the angle of reflection for the two bound particle shapes then we show the stationary distributions for speed.
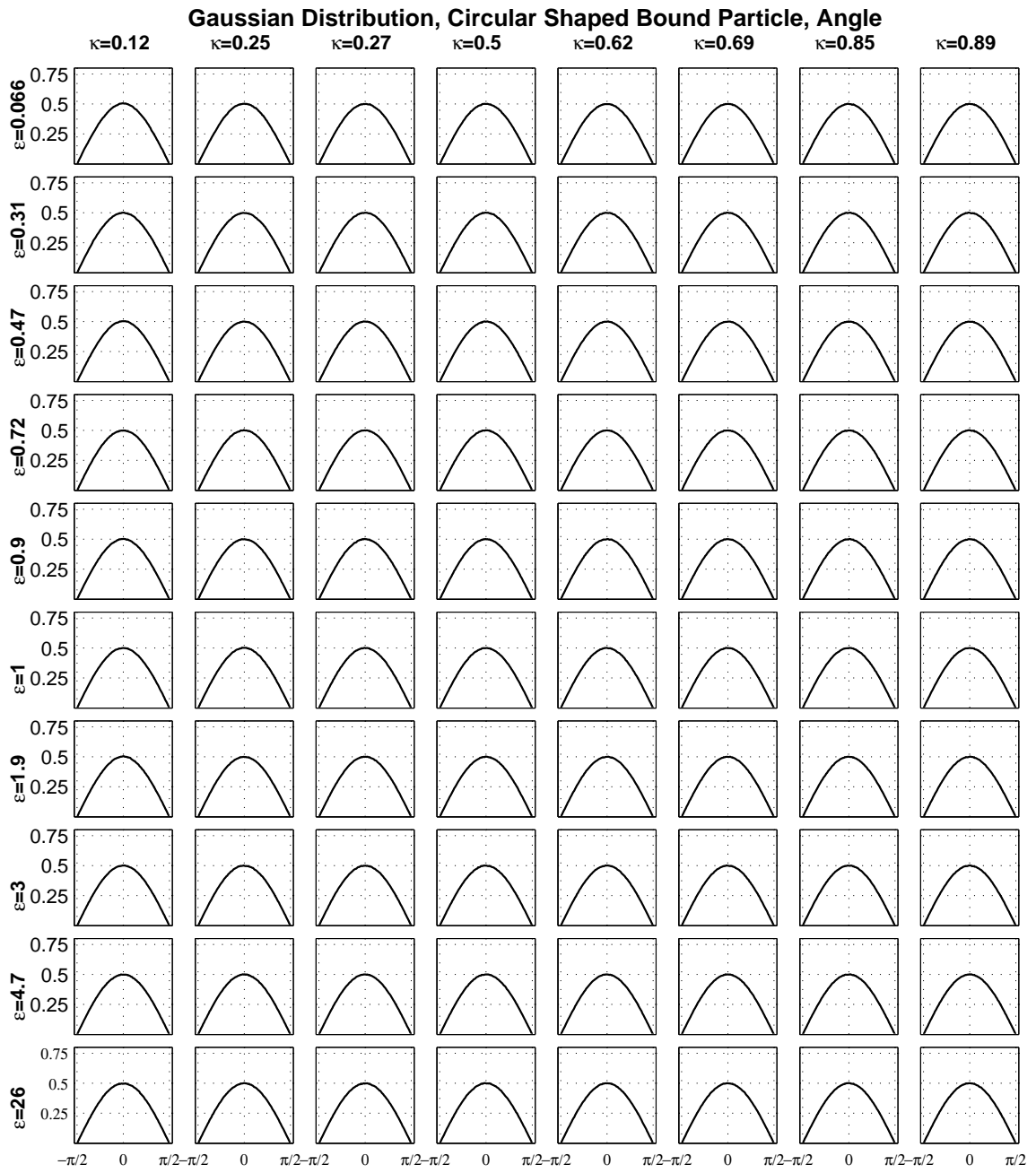
Figure 5.1. Gaussian Distribution, Circular Bound Particle, Angle of Reflection

88
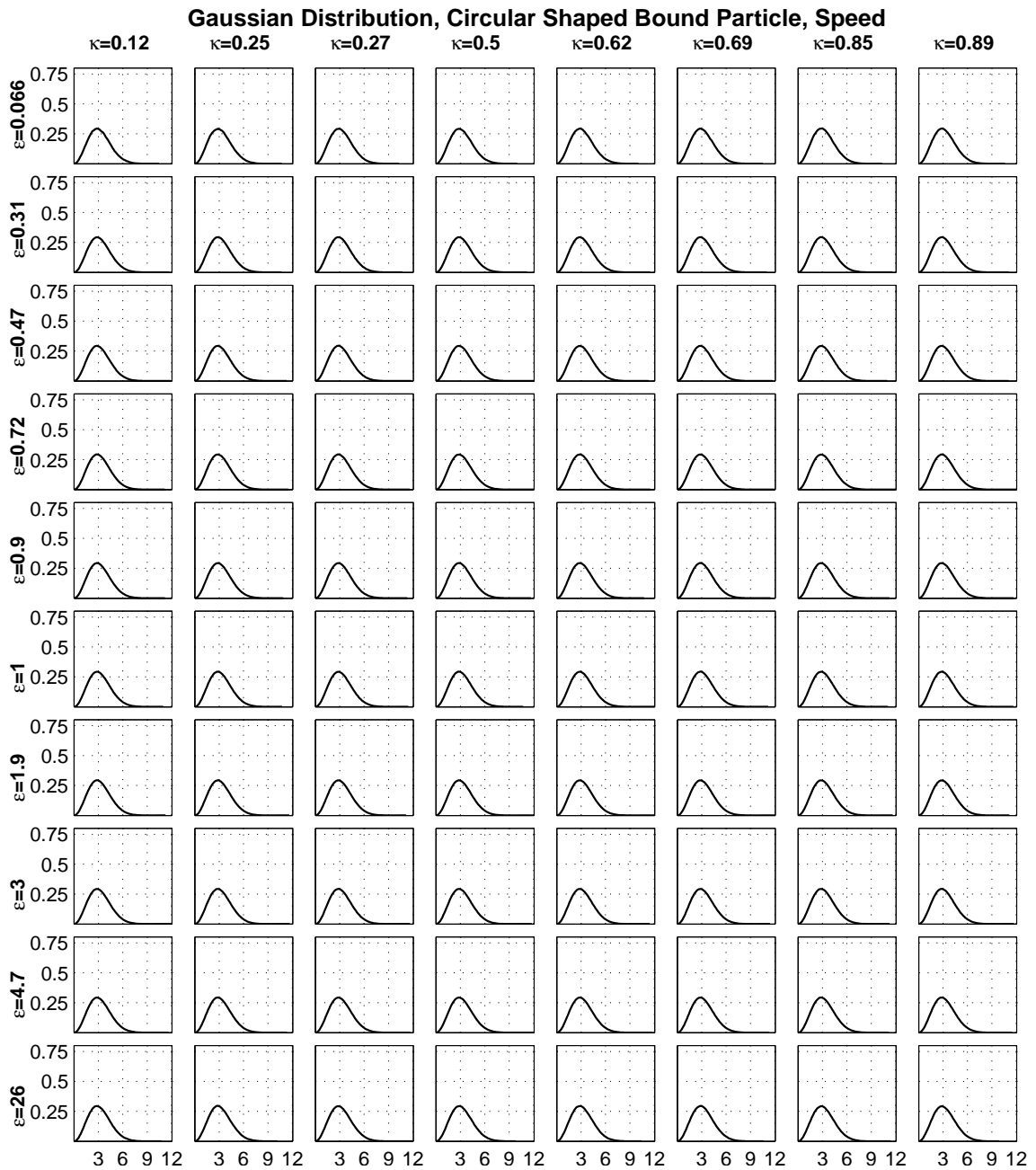
Figure 5.2. Gaussian Distribution, Circular Bound Particle, Speed

5.5 Spectral Gap

The simulation data also provides spectral information, under the assumption that these operators are compact. Below I have plotted spectral gap (the distance
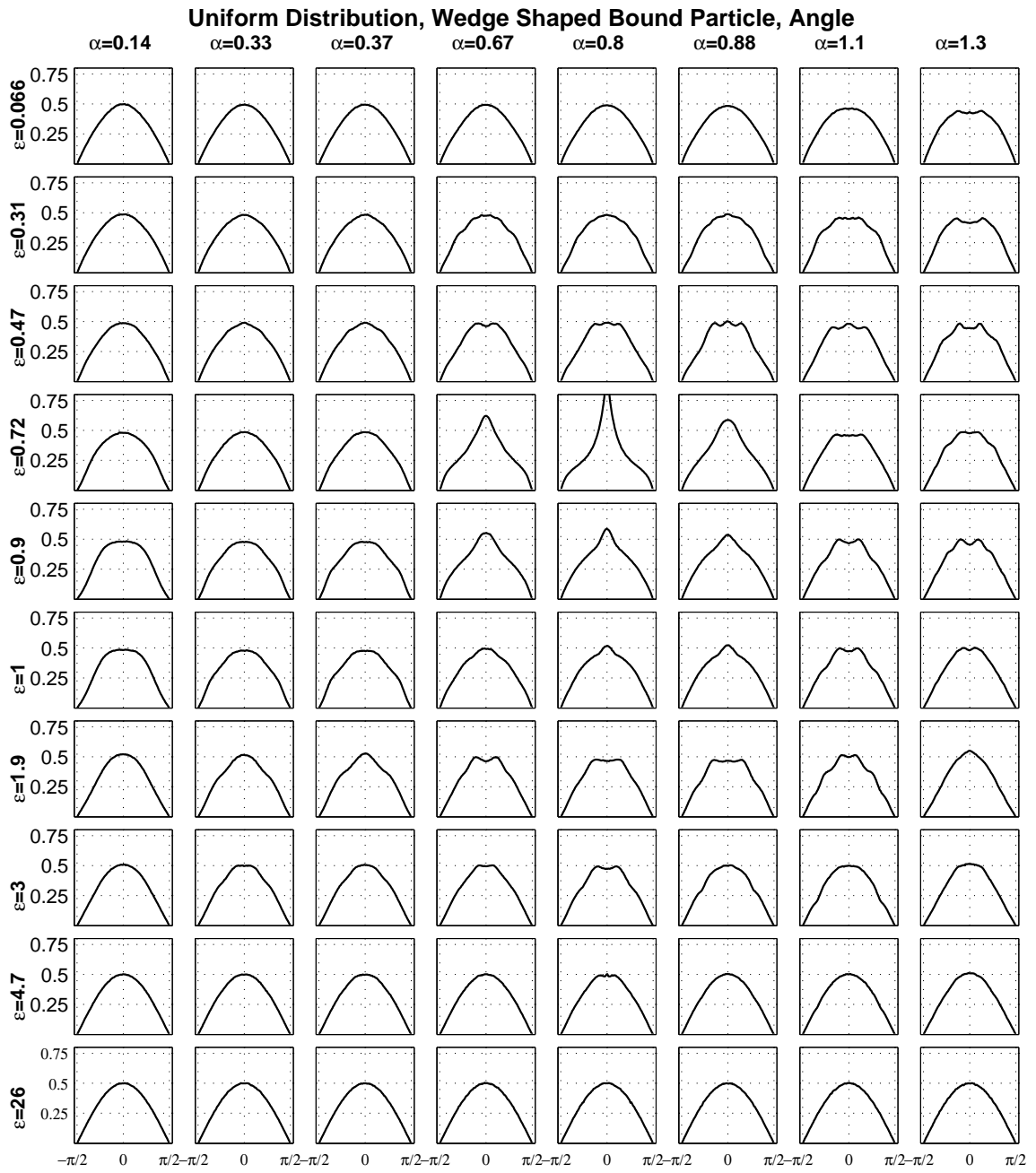
Figure 5.3. Uniform distribution, Wedge Shaped Bound Particle, Angle of Reflection
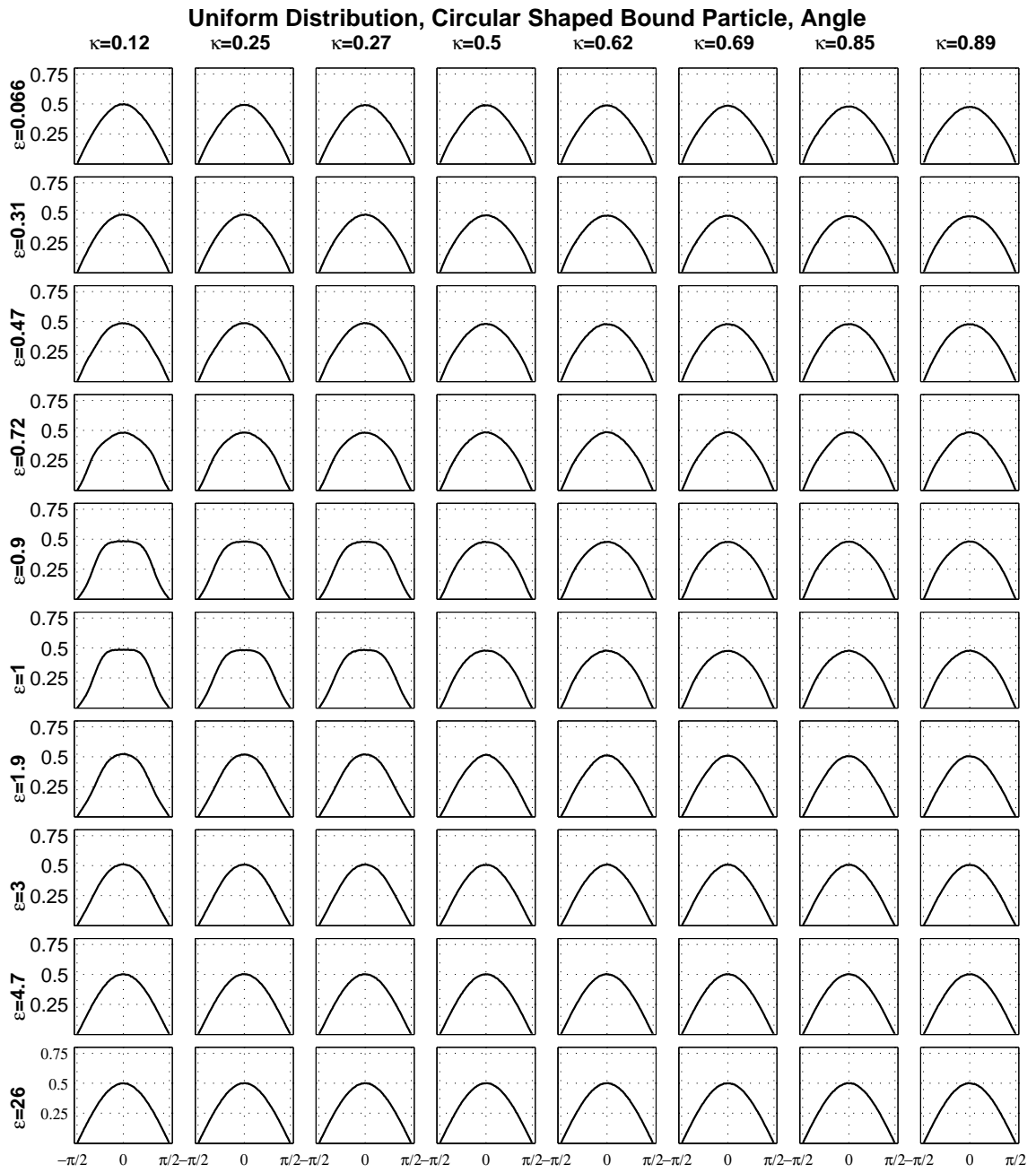
Figure 5.4. Uniform distribution, Circular Bound Particle, Angle of Reflection
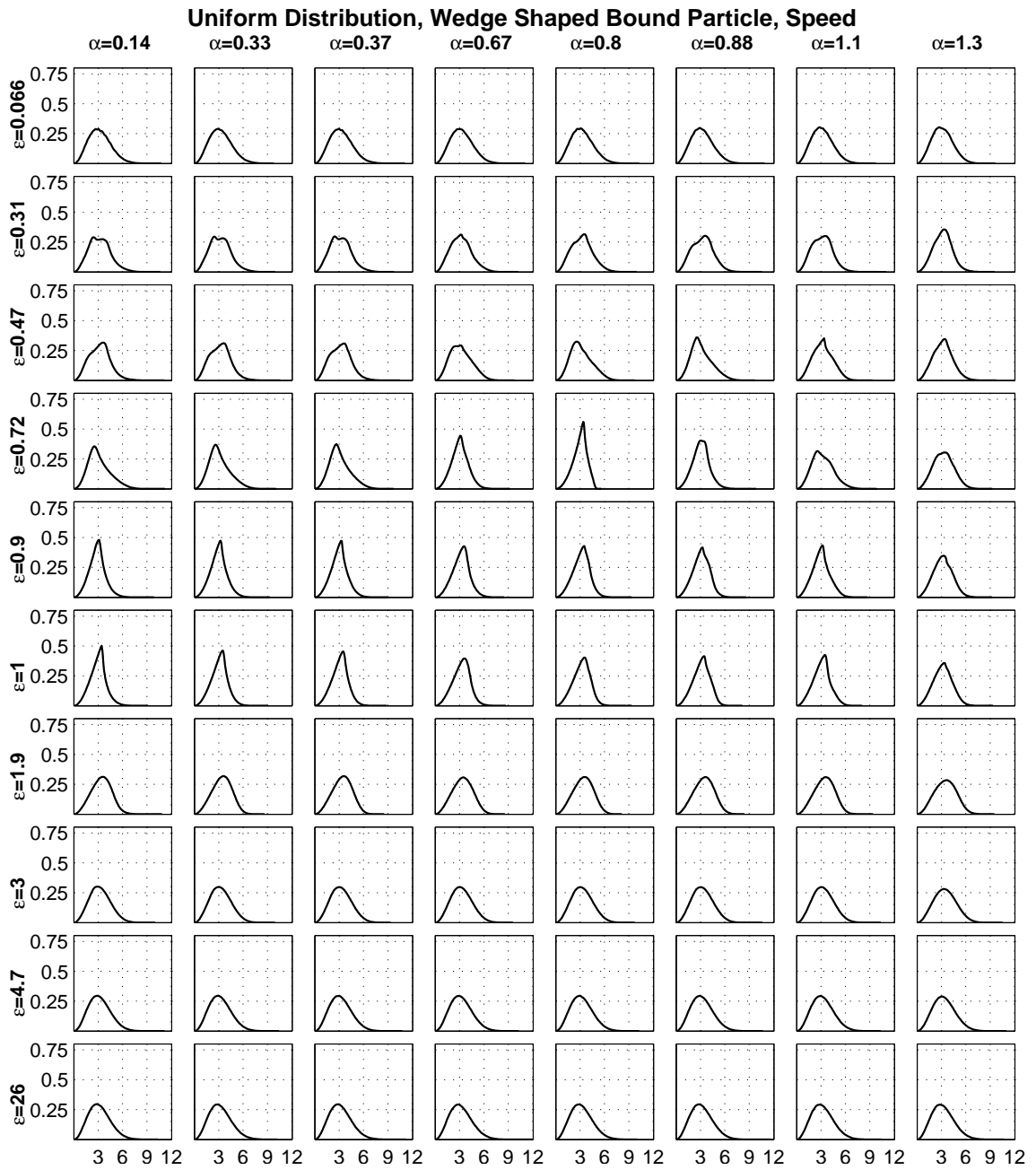
Figure 5.5. Uniform distribution, Wedge Shaped Bound Particle, Speed

between the largest eigenvalue 1 and the second largest eigenvalue). Spectral gap is commonly used to bound rates of convergence for Markov chains.

Uniform Distribution, Circular Shaped Bound Particle, Speed
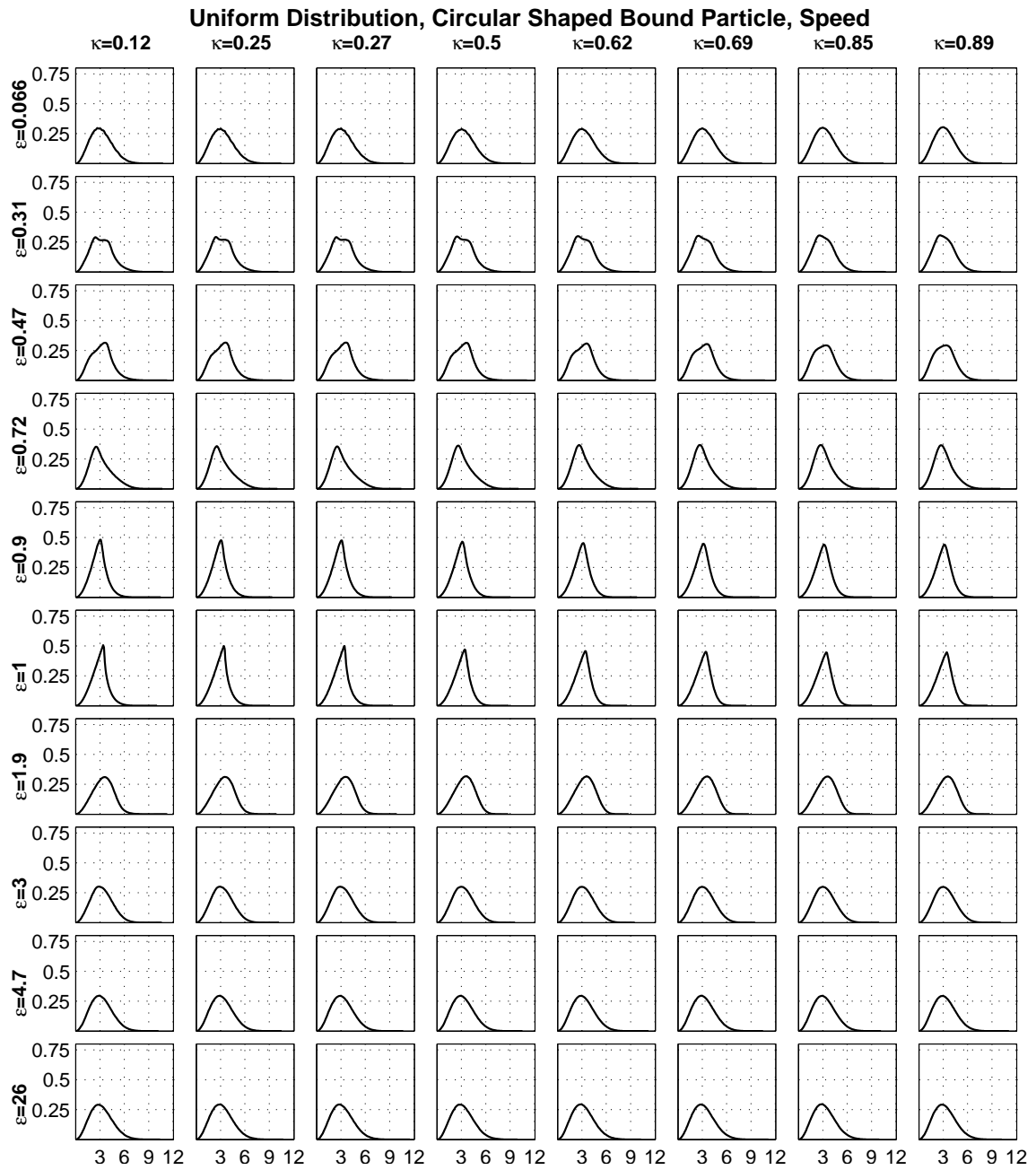
Figure 5.6. Uniform distribution, Circular Bound Particle, Speed

Since we have shown that the chain associated to Gaussian distribution of $\dot{x}$ is self-adjoint, all the plots below correspond to the Gaussian situation. For each pair (bound particle shape, kinetic variable), I have performed two types of experiments

93
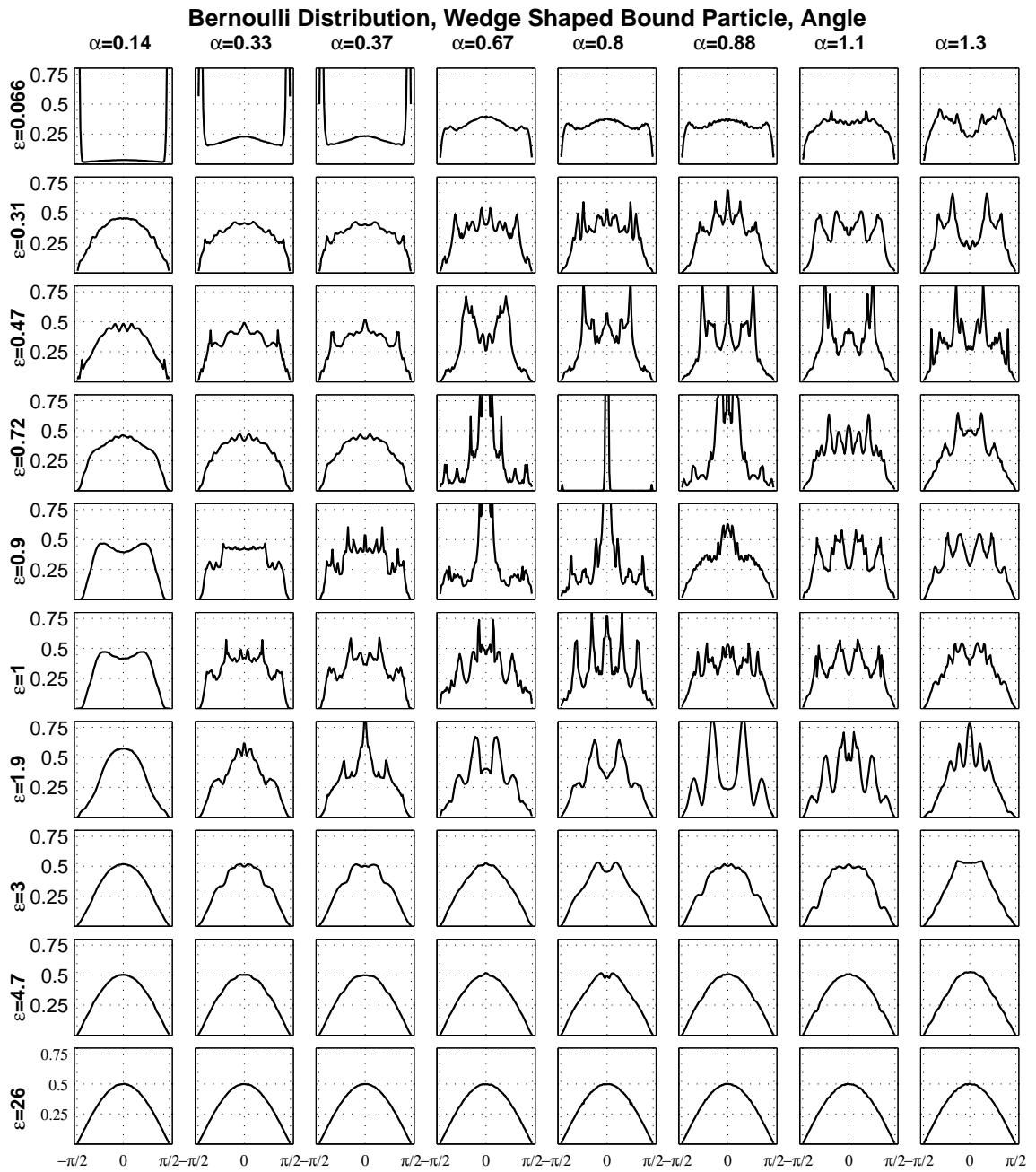
Figure 5.7. Bernoulli distribution, Wedge Shaped Bound Particle, Angle of Reflection
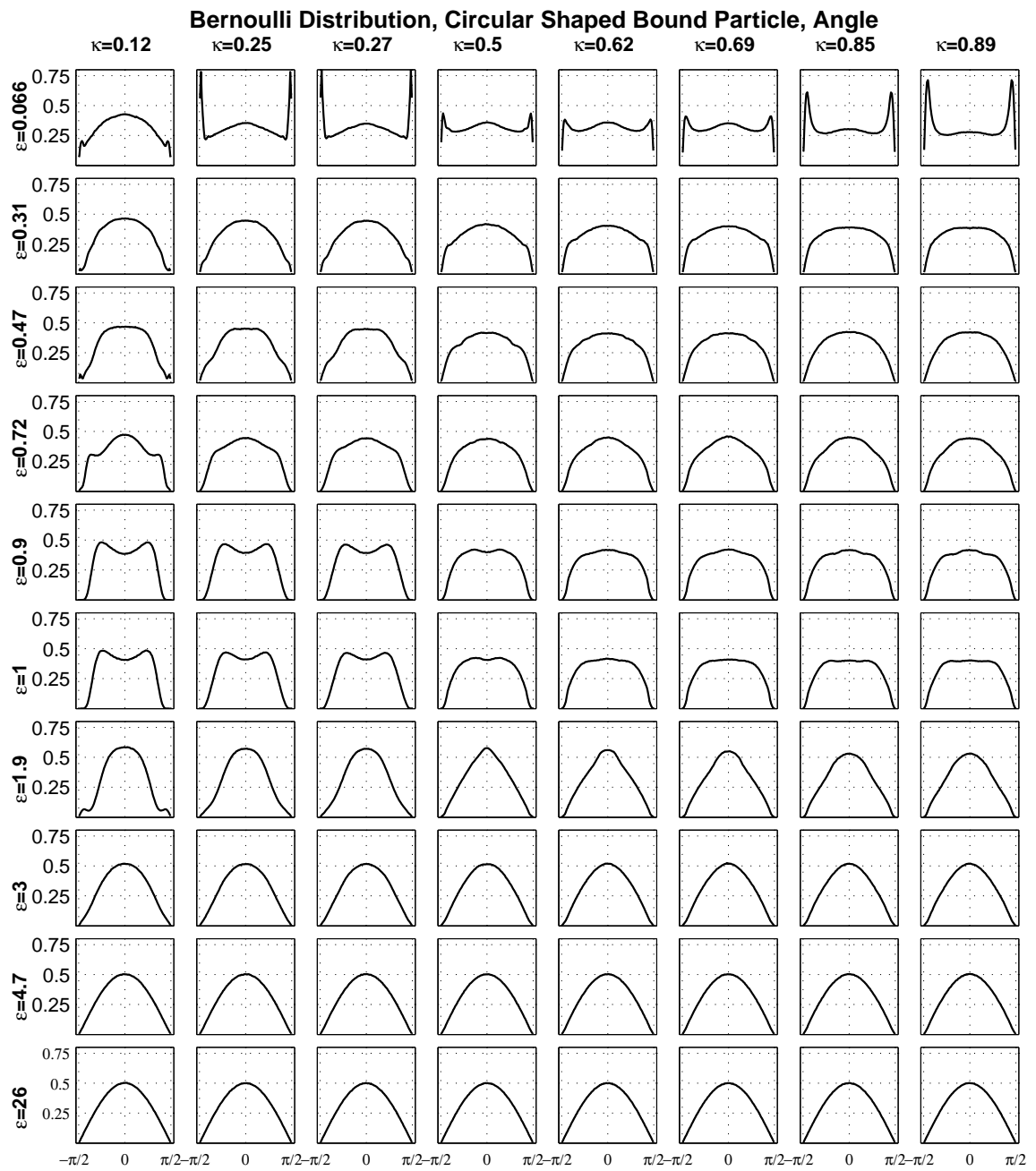
Figure 5.8. Bernoulli distribution, Circular Bound Particle, Angle of Reflection
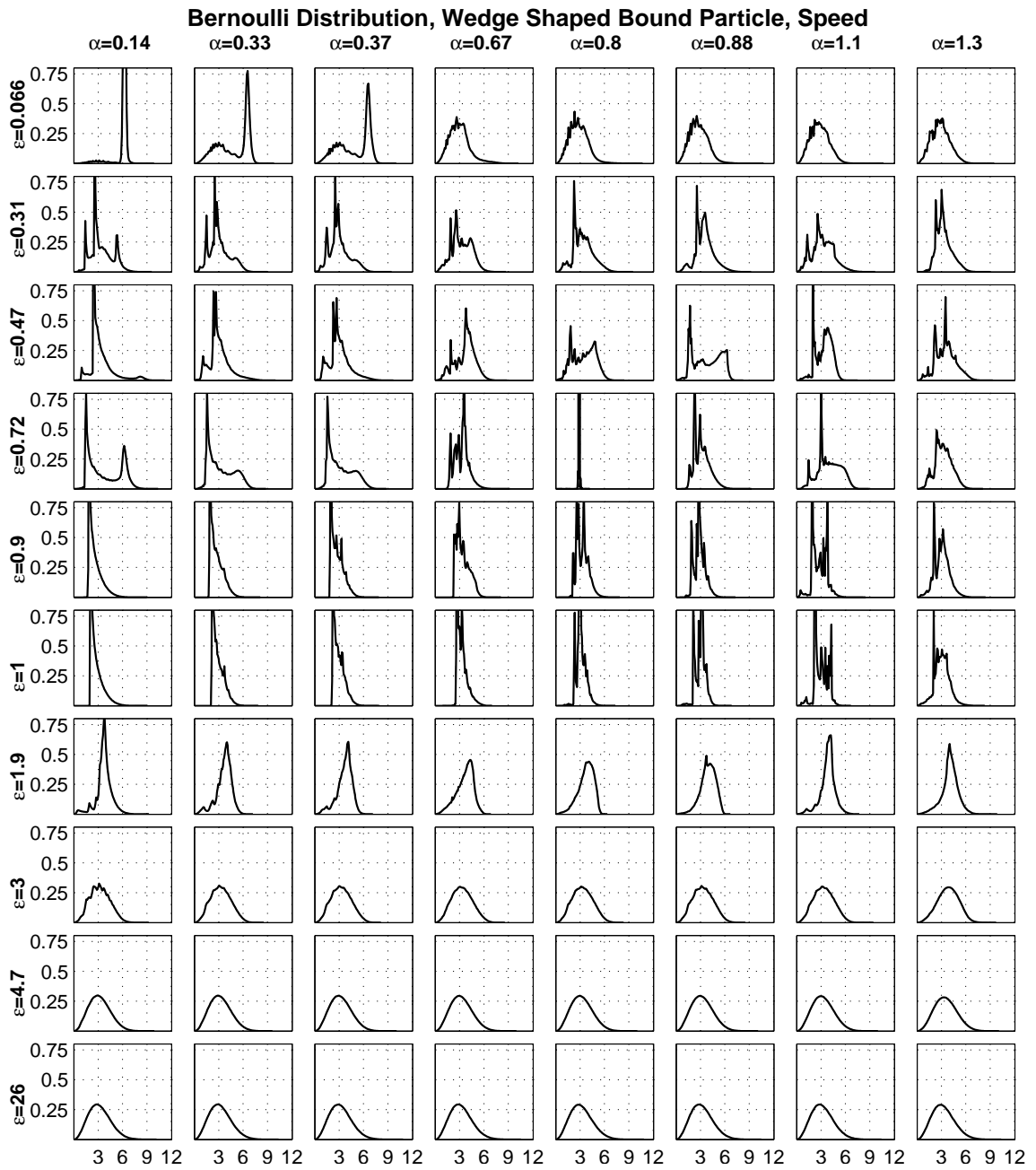
Figure 5.9. Bernoulli distribution, Wedge Shaped Bound Particle, Speed

1. Fix 4 values of the geometric parameter (either α or κ) and plot spectral gap versus ϵ

96
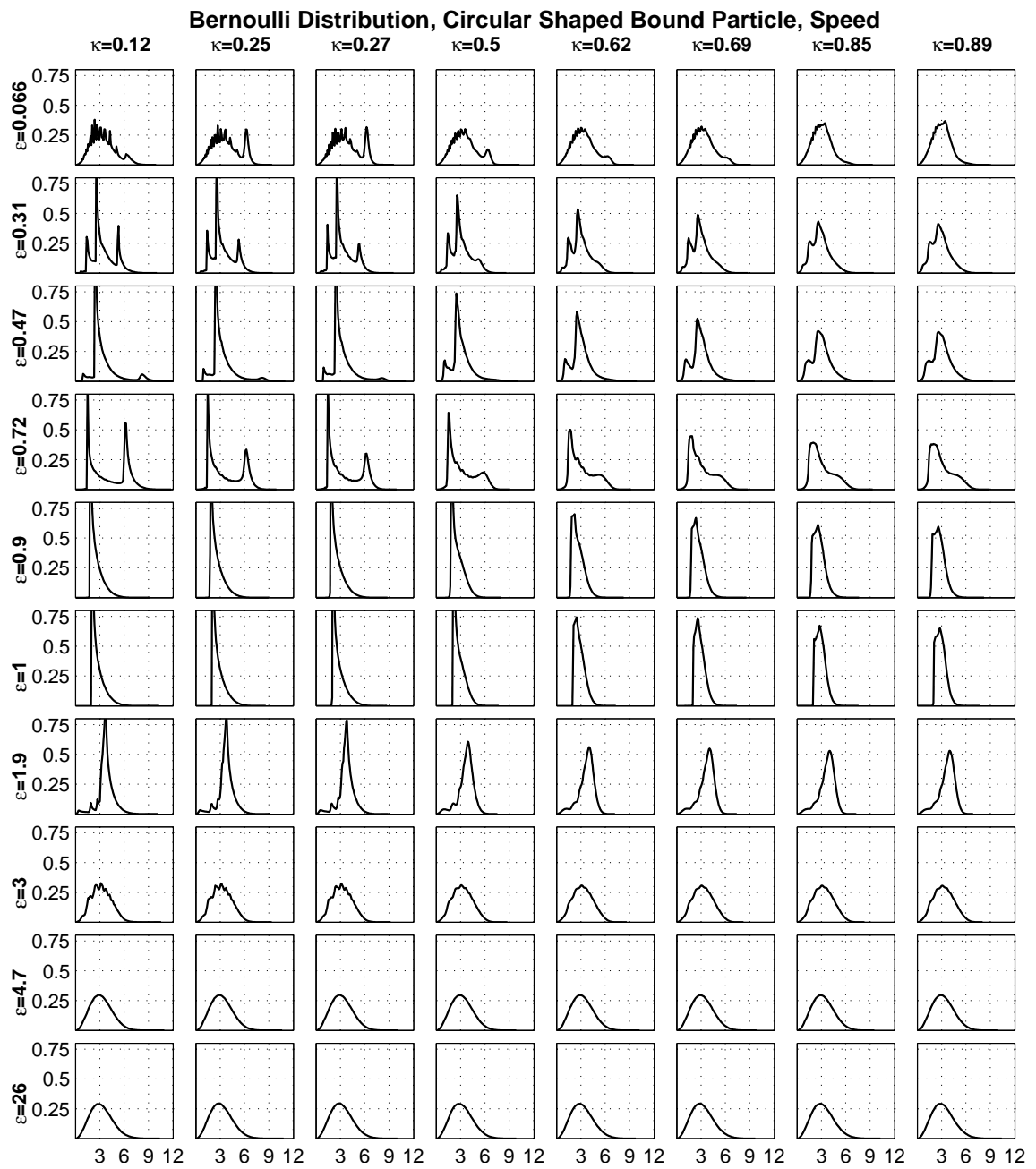
Figure 5.10. Bernoulli distribution, Circular Bound Particle, Speed

2. Fix 4 values of ϵ and plot spectral gap versus the geometric parameter (either α or κ)

Thank you for reading to the end. Or even if not, thank you for reading the last page.

Gaussian Distribution, Wedge Shaped Bound Particle, Angle Spectral Gap

Legend:
- $\alpha=0.07$
- $\alpha=0.16$
- $\alpha=0.18$
- $\alpha=0.34$

epsilon
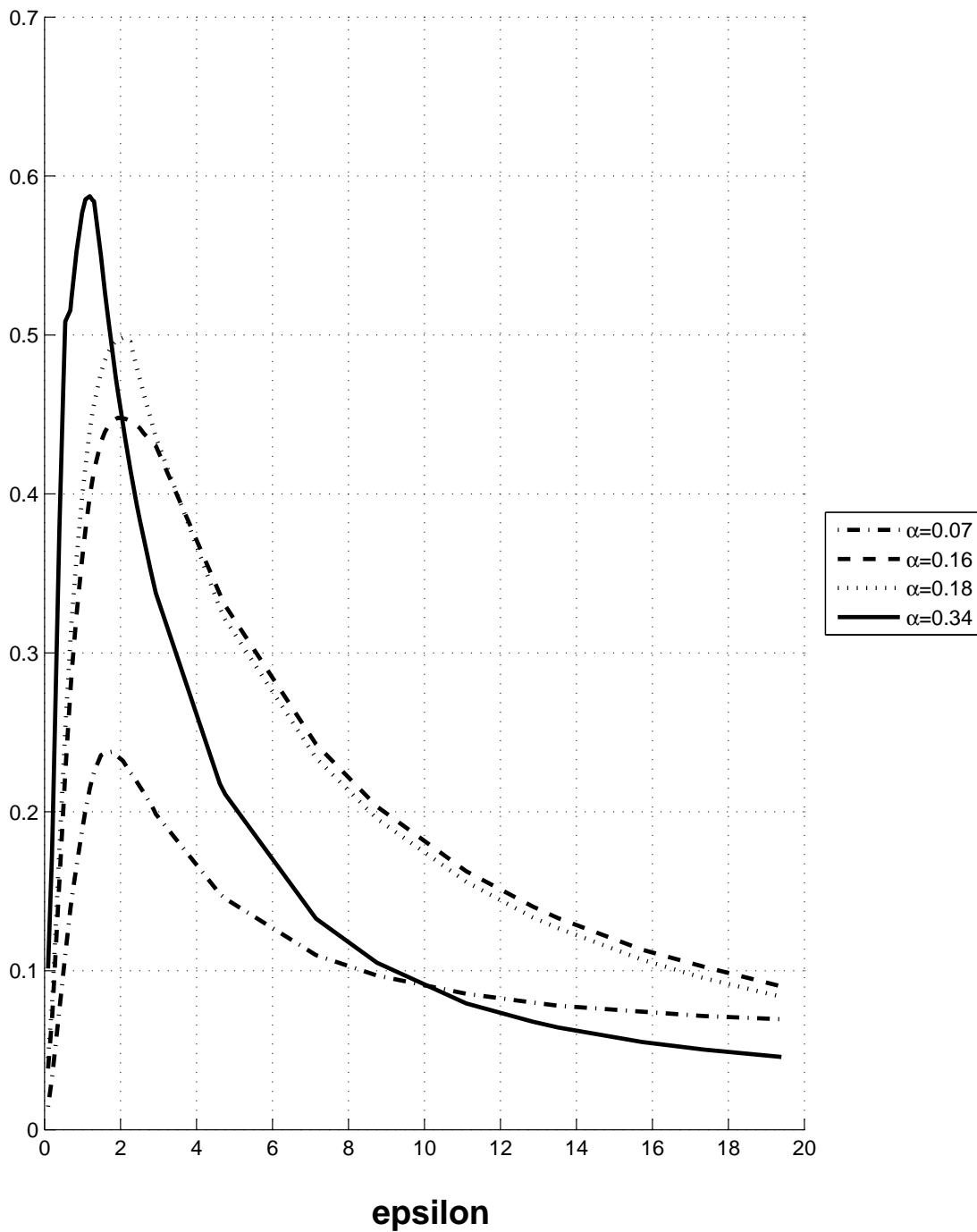
Figure 5.11. Gaussian distribution, Wedge Shaped Bound Particle, Angle, Spectral Gap for four fixed values of α

Gaussian Distribution, Wedge Shaped Bound Particle, Angle Spectral Gap
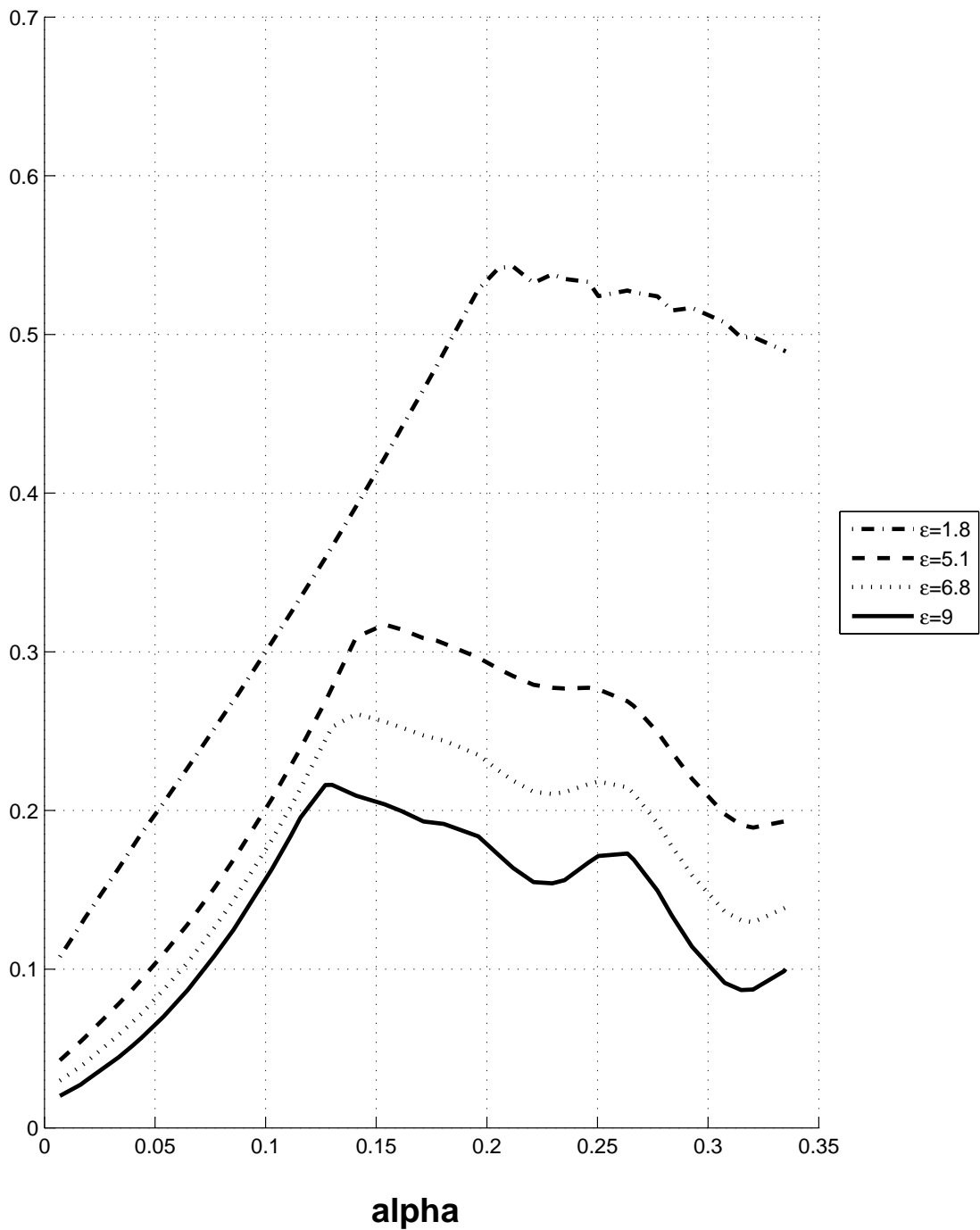
Figure 5.12. Gaussian distribution, Wedge Shaped Bound Particle, Angle, Spectral Gap for four fixed values of ϵ
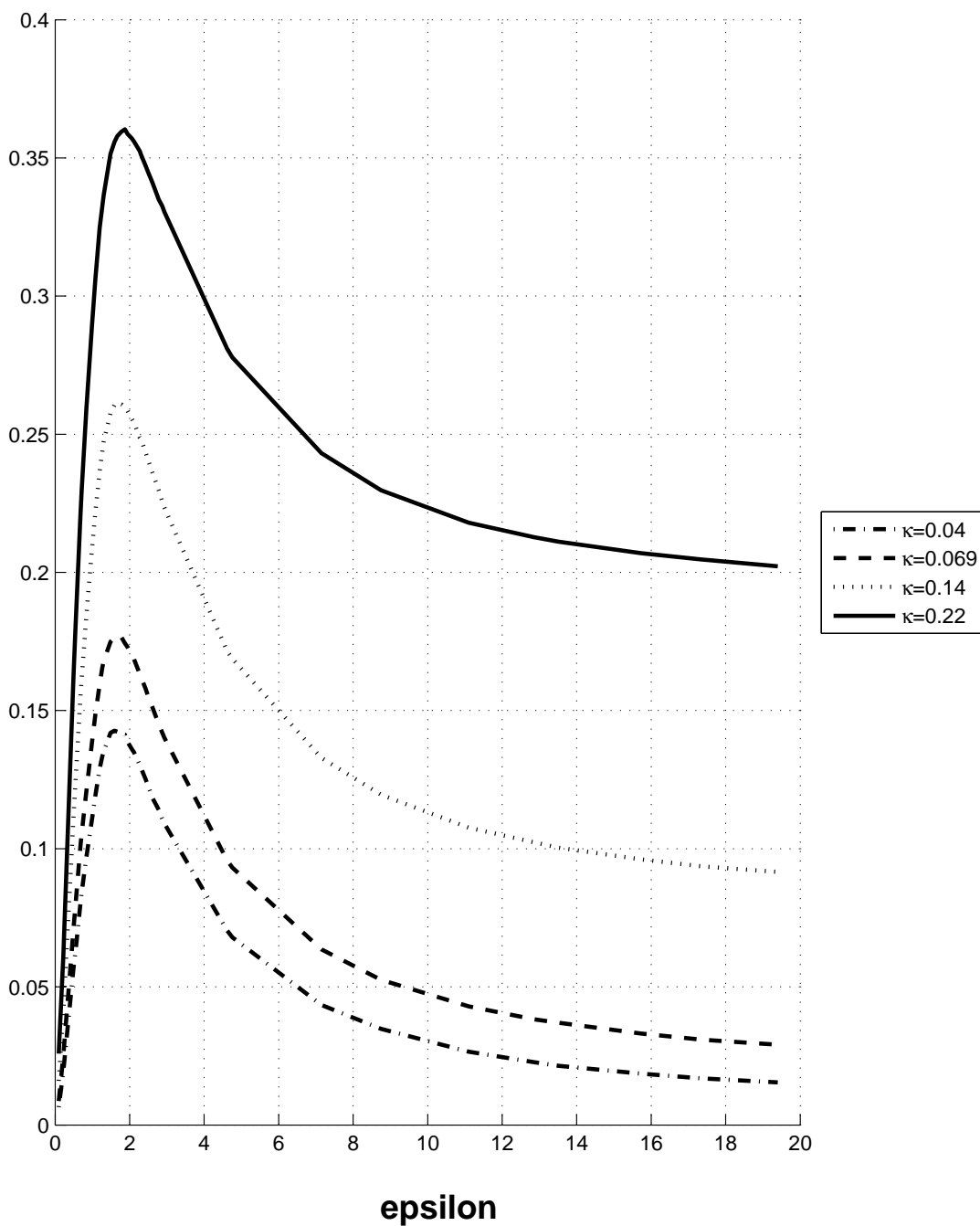
Figure 5.13. Gaussian distribution, Circular Shaped Bound Particle, Angle, Spectral Gap for four fixed values of κ

Gaussian Distribution, Circular Shaped Bound Particle, Angle Spectral Gap
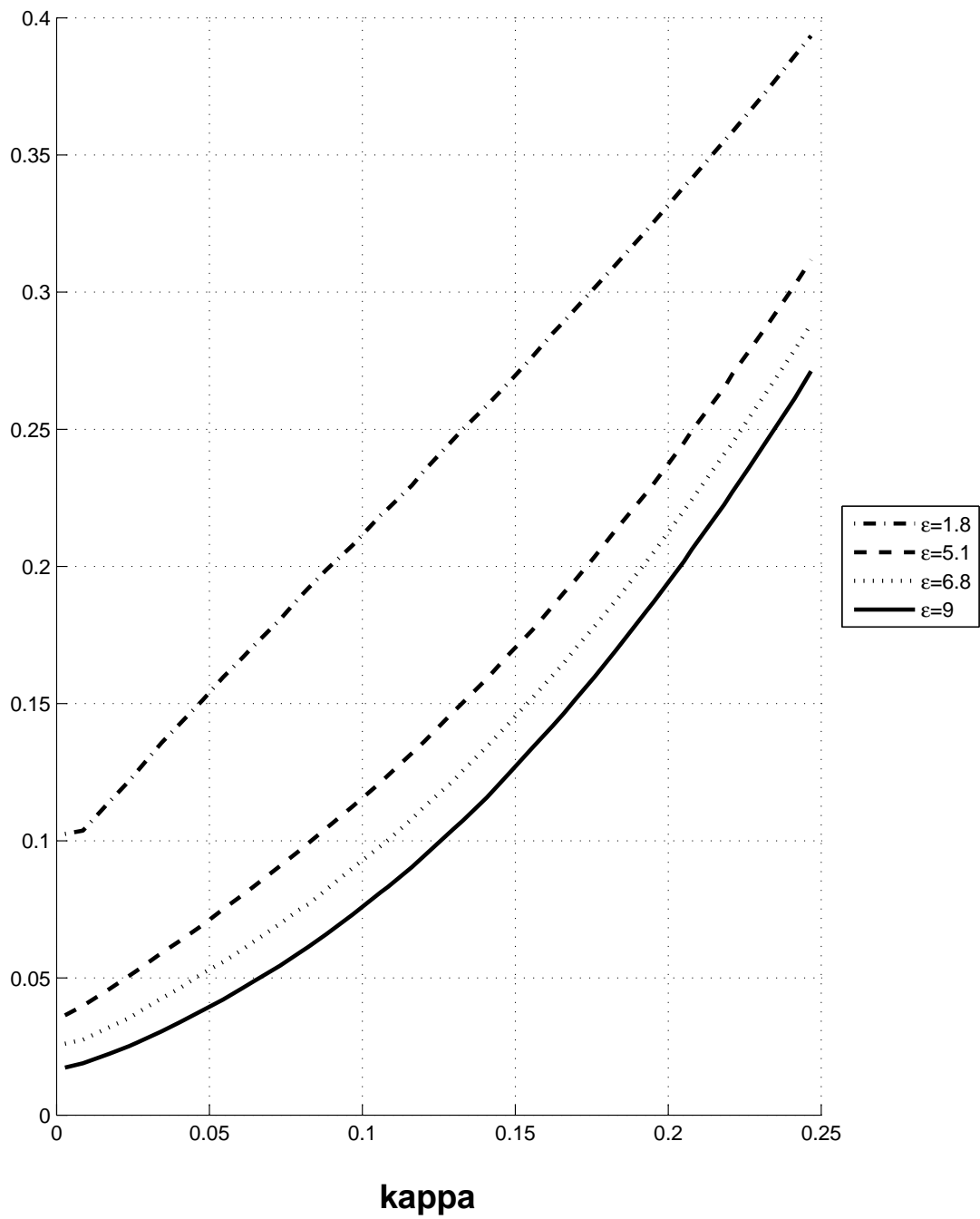
Figure 5.14. Gaussian distribution, Circular Shaped Bound Particle, Angle, Spectral Gap for four fixed values of ϵ

Gaussian Distribution, Wedge Shaped Bound Particle, Speed Spectral Gap
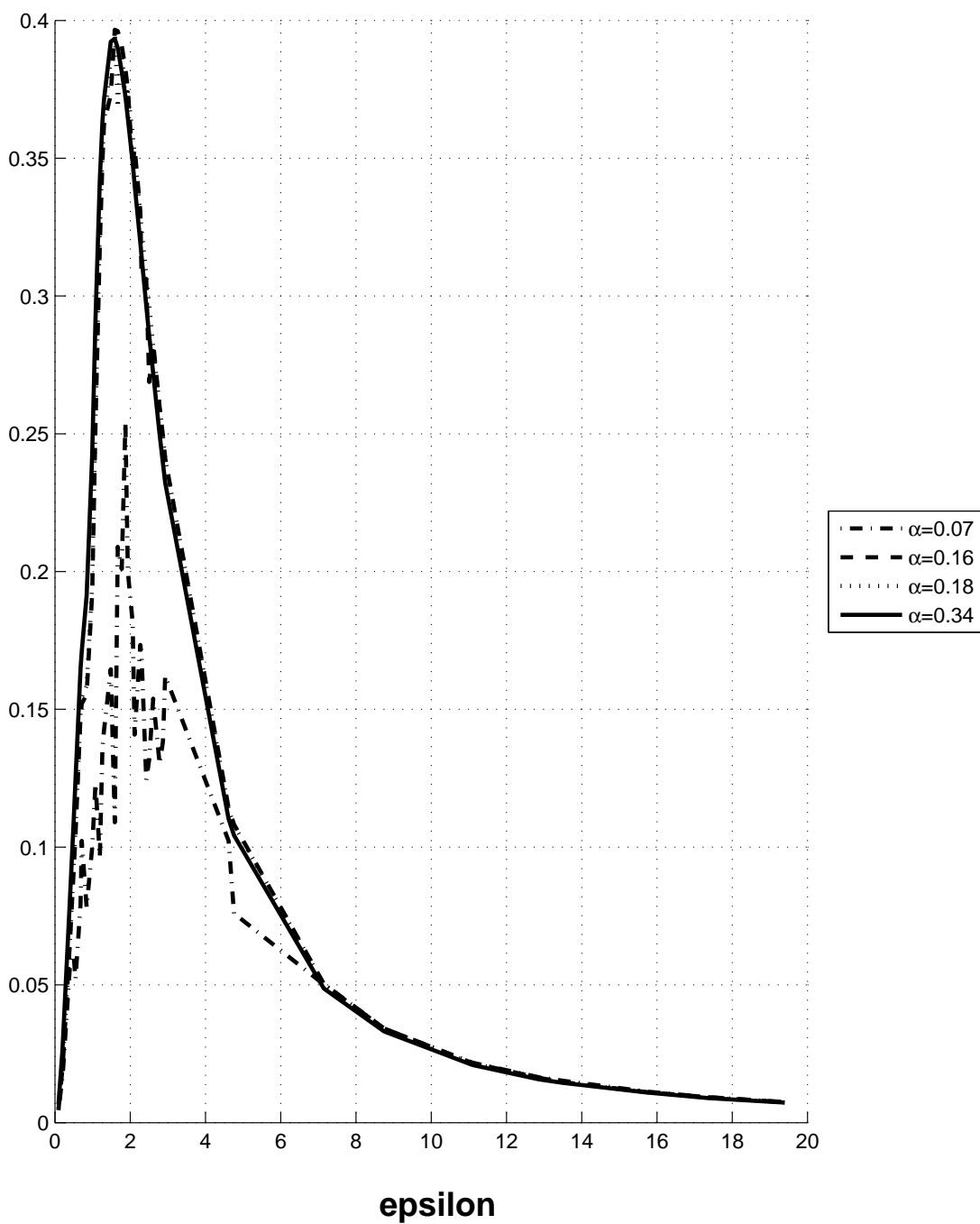
Figure 5.15. Gaussian distribution, Wedge Shaped Bound Particle, Speed, Spectral Gap for four fixed values of α
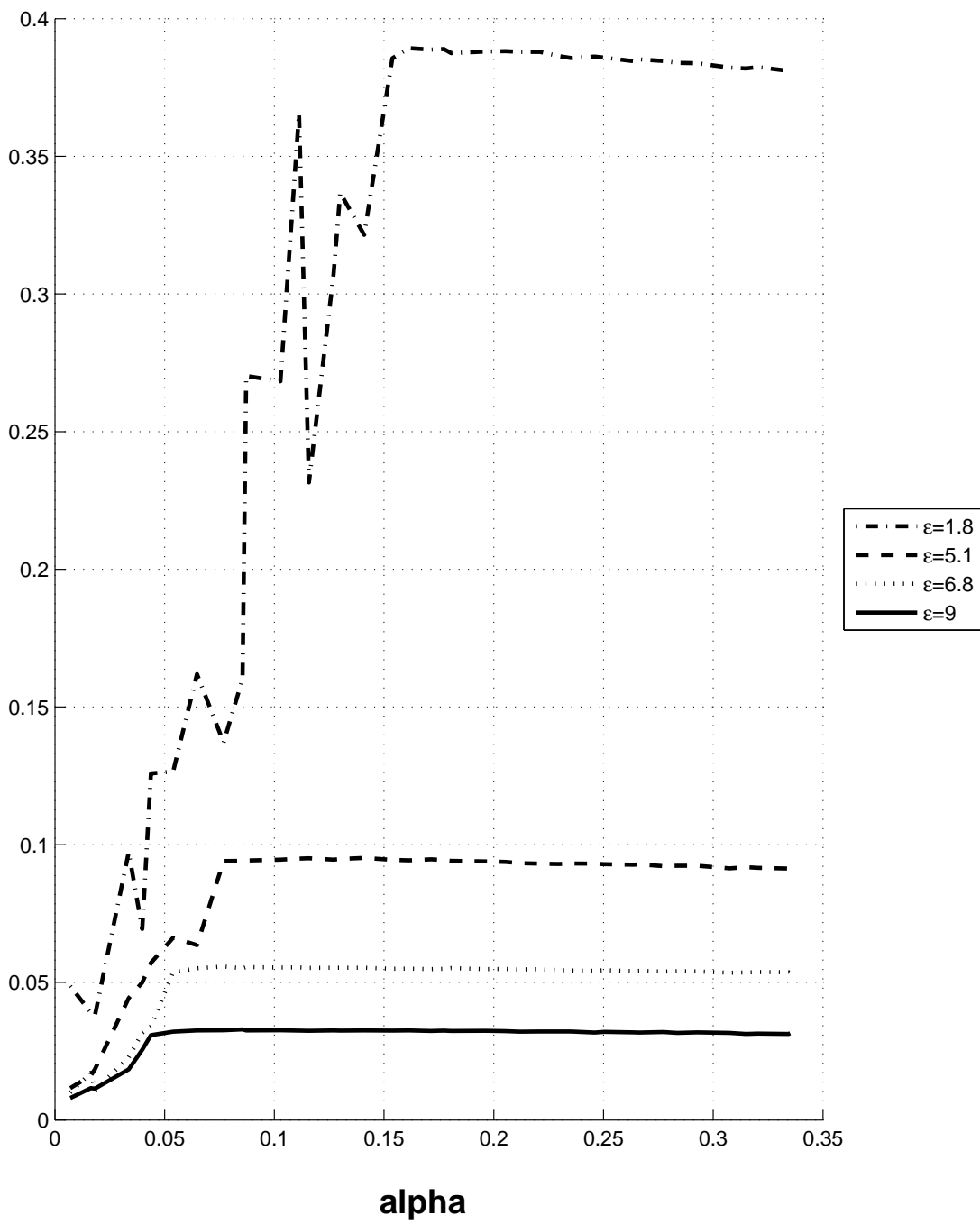
Figure 5.16. Gaussian distribution, Wedge Shaped Bound Particle, Speed, Spectral Gap for four fixed values of ϵ
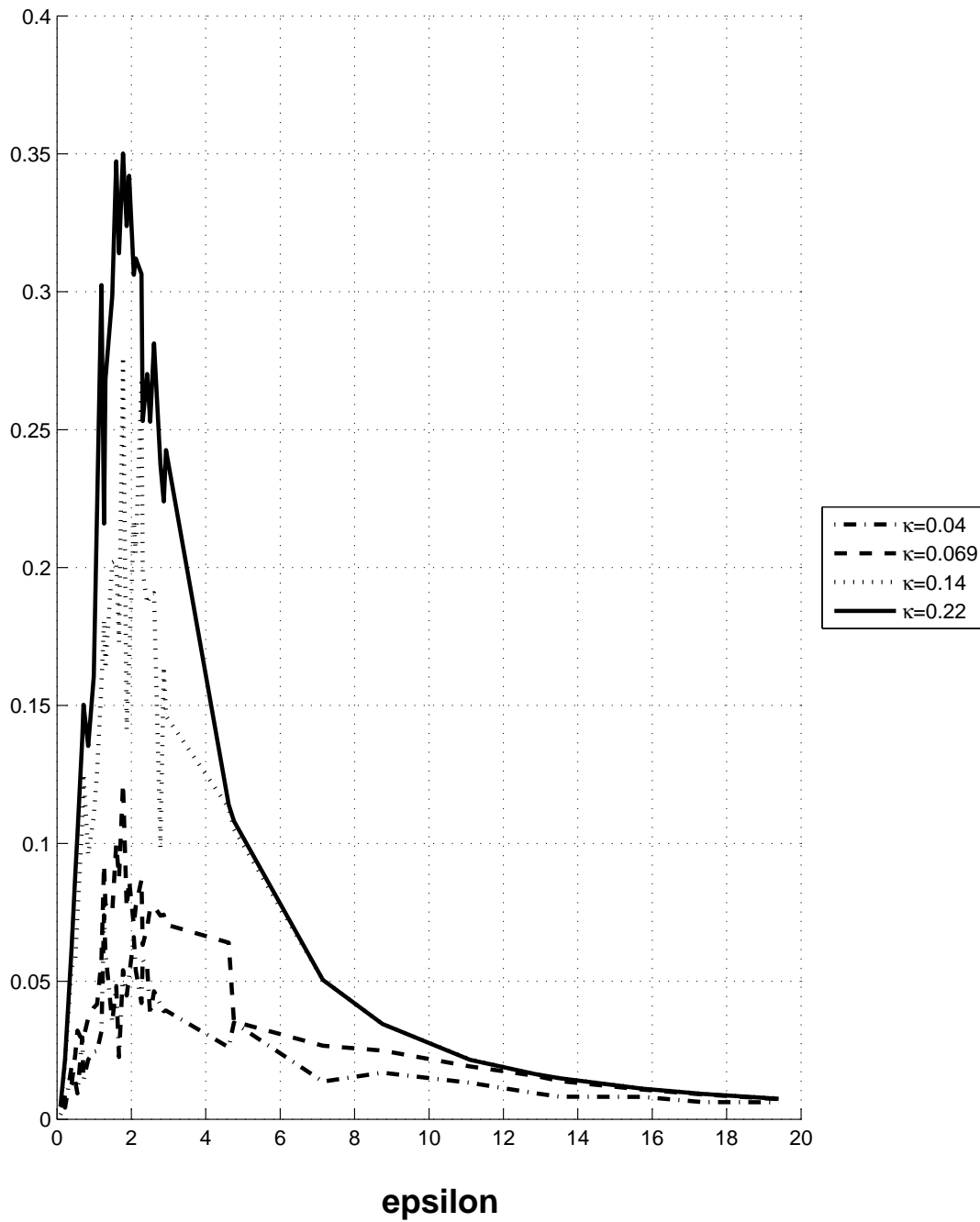
Figure 5.17. Gaussian distribution, Circular Shaped Bound Particle, Speed, Spectral Gap for four fixed values of κ

Gaussian Distribution, Circular Shaped Bound Particle, Speed Spectral Gap
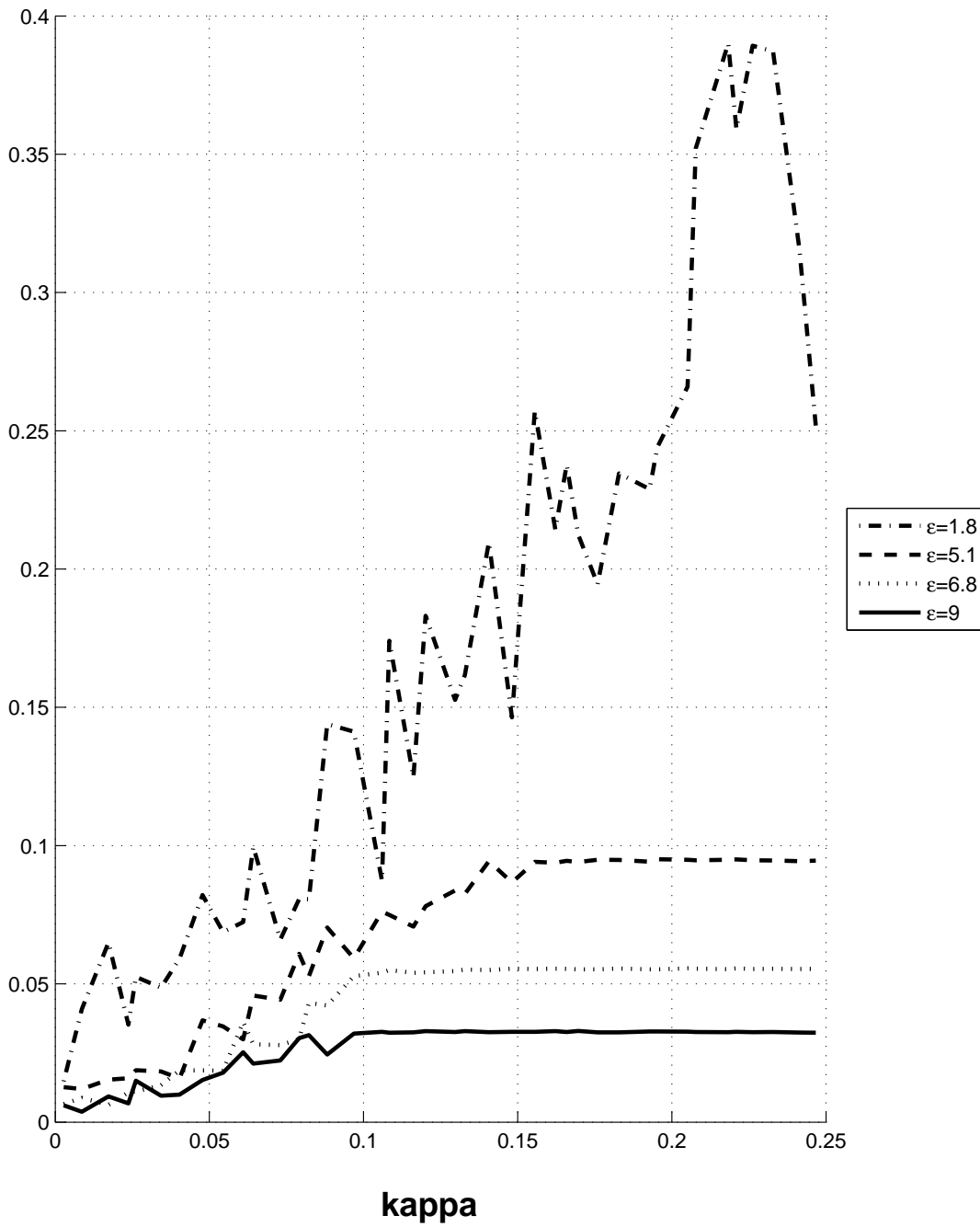
Figure 5.18. Gaussian distribution, Circular Shaped Bound Particle, Speed, Spectral Gap for four fixed values of ϵ

REFERENCES

[1] R Feres and H Zhang. The spectrum of the billiard Laplacian of a family of random billiards. *Journal of Statistical Physics*, 141:1039–1054, 2010. 10.1007/s10955-010-0079-5.

[2] D Levin, Y Peres, and E Wilmer. *Markov Chains and Mixing Times.* American Mathematical Society, Providence, RI, 2000.

[3] D Bayer and P Diaconis. Trailing the dovetail shuffle to its lair. *Ann. Appl. Probab.*, 2(2):294–313, 1992.

[4] Kenneth S. Brown and Persi Diaconis. Random walks and hyperplane arrangements. *Ann. Probab.*, 26(4):1813–1854, 1998.

[5] J Marsden and T Ratiu. *Introduction to mechanics and symmetry : a basic exposition of classical mechanical systems.* Springer, New York, 1999.

[6] N Chernov and R Markarian. *Chaotic Billiards.* American Mathematical Society, Providence, RI, 2006.

[7] R Feres and G Yablonsky. Knudsen's cosine law and random billiards. *Chemical Engineering Science*, 59(7):1541–1556, APR 2004.

[8] R Feres. Random walks derived from billiards. *Dynamics, ergodic theory, and geometry*, 54:179–222, 2007.

[9] C Cercignani. *The Boltzmann equation and its applications*, volume 67. Springer-Verlag, New York, 1988.